

# Nymeria: A Massive Collection of Multimodal Egocentric Daily Motion in the Wild

Lingni Ma<sup>1</sup>, Yuting Ye<sup>1</sup>, Fangzhou Hong<sup>2</sup>, Vladimir Guzov<sup>3</sup>, Yifeng Jiang<sup>4</sup>,  
Rowan Postyeni<sup>1</sup>, Luis Pesqueira<sup>1</sup>, Alexander Gamino<sup>1</sup>, Vijay Baiyya<sup>1</sup>,  
Hyo Jin Kim<sup>1</sup>, Kevin Bailey<sup>1</sup>, David S. Fosas<sup>1</sup>, C. Karen Liu<sup>4</sup>, Ziwei Liu<sup>2</sup>,  
Jakob Engel<sup>1</sup>, Renzo De Nardi<sup>1</sup>, and Richard Newcombe<sup>1</sup>

<sup>1</sup> Meta Reality Labs Research

<sup>2</sup> Nanyang Technological University

<sup>3</sup> University of Tübingen

<sup>4</sup> Stanford University

<https://www.projectaria.com/datasets/nymeria>

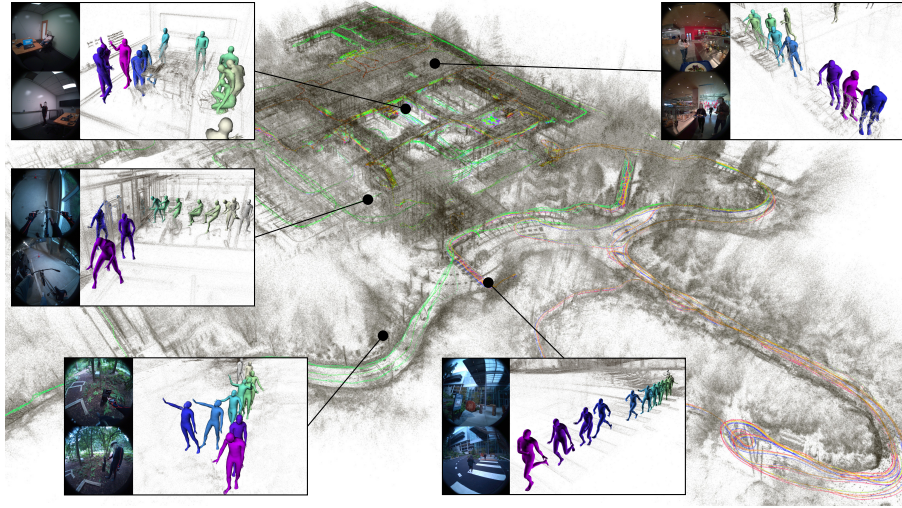


**Fig. 1: A glimpse of Nymeria dataset.** The figure shows example indoor and outdoor activities captured on a campus, where the point clouds and trajectories are the SLAM output by tracking all egocentric devices *i.e.* the glasses and wristbands. Each sub-figure is a motion clip from a different participant, where the top left gives the latest egocentric view, the right is the 3D localized full-body motion synchronized with the headset and the bottom left provides an auxiliary third-person view.

**Abstract.** We introduce Nymeria - a large-scale, diverse, richly annotated human motion dataset collected in the wild with multiple multimodal egocentric devices. The dataset comes with a) full-body 3D motion ground truth; b) egocentric multimodal recordings from Project Aria devices with RGB, grayscale and eye-tracking cameras, IMUs, magnetometer, barometer, and microphones; and c) an additional "observer"

device providing a third-person viewpoint. We compute world-aligned 6DoF transformations for all sensors, across devices and capture sessions. The dataset also provides 3D scene point clouds and calibrated eye gaze. We derive a protocol to annotate hierarchical language descriptions of in-context human motion, from fine-grain pose narrations, to atomic actions and coarse activity summarization. To the best of our knowledge, the Nymeria dataset is the world’s largest in-the-wild collection of human motion with natural and diverse activities; first of its kind to provide synchronized and localized multi-device multimodal egocentric data; and the world’s largest dataset of motion with language descriptions. It contains 1200 recordings totalling 300 hours of daily activities of 264 participants across 50 locations, travelling a total of 399Km . The motion-language descriptions provide 310.5K sentences in 8.64M words from a vocabulary size of 6545. To demonstrate the potential of the dataset we define key research tasks for egocentric body tracking, motion synthesis, and action recognition and evaluate several state-of-the-art baseline algorithms. Data and code will be open-sourced.

**Keywords:** motion capture · egocentric · multimodal · large dataset

## 1 Introduction

The advent of AI is leading to a surge of smart glasses [1–5, 8, 10, 27] and other AI enabled wearable device applications. These devices not only provide seamless access to LLM-based AI assistants, but also are multi-modal data-capture vehicles that can capture immediate and long-term personalized context, allowing such AI assistants to evolve into the next generation of human-centric, contextualized AI and – long-term – combined with AR/VR technology to unlock a new generation of *contextualized computing*.

Important context includes the wearer’s own motion (ego-motion) and their actions. Reliably estimating this context solely from body-worn devices is very challenging as typically the sensor measurements alone are insufficient to fully constrain the full body pose – requiring the use of generative methods and techniques from the field of full body motion synthesis. In practice, most research in this direction is severely limited by the existing training data, having to rely on either simulations that lack realism and completeness [11, 12, 40, 41, 47, 85], or limited data collections lacking scale and diversity [34, 44–46, 66, 90]. There are three key technical challenges:

- *Obtaining full-body motion ground truth.* Vision-based solutions such as the ones relying on optical markers [44, 58, 66] or multi-view videos [30, 43, 50, 96] are adversely affected by line-of-sight visibility, and require a complex multi-camera-setup to cover a limited range of motions inside a constrained volume. Inertial-based solutions [6, 9] are an alternative, but suffer from accumulation of error and thus are inferior in global accuracy [59, 78].
- *Multi-device synchronization.* Combining multiple capture devices or ground-truth systems requires accurate time- and 6DoF-alignment, which can be



challenging when using off-the-shelf solutions that cannot be modified or can lack support for universal protocols. Instead, most existing datasets work around this problem using visual cues [30, 43, 96] or audio [34] signals. However, such approaches are limited in accuracy and reliability. Especially for long recordings, clock-drift accumulates and these methods become intrusive and interrupting to the activity. Consequently, the average motion length is very short for existing datasets (*cf.* Tab. 2).

- *Data processing and annotations.* These are critical for a dataset to develop its full potential. In addition to the raw body motion, multi-device co-localization and 3D scene representation, we believe natural language descriptions are crucial for future research directions. Existing work provides simple descriptions without scene context [23, 31, 71], which is typically done by playing back motion clips for annotators in isolation. Compared to the text corpus for training LLMs [13, 65, 86], the scale of motion-language dataset is significantly smaller.

To fill the gap and accelerate the research, we introduce the Nymeria dataset: the world largest collection of in-the-wild human motion with rich, multimodal egocentric captures and annotations. Tab. 1 summarizes the core statistics of our dataset. It contains 300 hours with 260M poses of 264 participants across 50 locations. Focusing on daily activities, we designed 20 indoor and outdoor scenarios to capture the diversity and authenticity of how people interact with the environments and others, *e.g.* playing games/sports with friends, dinning in the cafeteria, working in the office, hiking in the woods, biking on the road etc. All recordings are 15 minutes long, providing ample time for natural activities with spontaneous, unscripted actions and interactions.

We use an inertial-based XSens Mocap [6] suite to capture full-body motion. We use Project Aria [27] glasses in all recordings to collect RGB, grayscale and eye tracking (ET) videos, multichannel audio and, raw data from inertial measurement units (IMUs), magnetometer and barometer. Similar multimodal data from both wrists is collected with a wristband device (miniAria) constructed by repackaging the electronics and sensors from Project Aria glasses to be wrist-worn. A non-intrusive custom hardware solution is used to achieve sub-millisecond time-synchronization across all devices and over the duration of each sessions. We use Project Aria Machine Perception Service (MPS) [7] to obtain accurate 6DoF device trajectories for headset and wristbands, 3D semi-dense

Seq	Qty	Ppl	Scn	Loc	Pose	Img	IMU	Gaze	Traj	Sent	Word	Voc
1200	300h	264	20	50	260M	201M	11.7B	10.8M	399Km	310.5K	8.64M	6545

**Table 1: Unprecedented scale of Nymeria dataset.** We capture 1200 sequences of 300 hours daily activity from 264 people, 50 locations with 20 scenarios in the wild. The data provides 260M body poses, 201.2M images, 11.7B IMU samples, 10.8M gazes. The head moving trajectory exceeds 399Km. The motion-language descriptions provide 310.5K sentences in 8.64M words from a vocabulary size of 6545.

dataset	q/h	p/M	$\mu$ /m	pp	nl/K	voc	pm	hd	3p	wd	ga	od	gz	sr	mp	hh
AMASS [58]	42	0.9	0.22	346			✓									
HPS [34]	4.5	0.5	8.2	7			✓	✓			✓	✓		✓	✓	✓
EgoBody [96]	2	0.4	1	36			✓	✓	✓				✓	✓	✓	✓
HML3D [31]	28.6	2.9	0.12	-	45.0	5371	✓									
EgoHuman [43]	3.5	0.4	0.5	7			✓	✓	✓			✓			✓	✓
MotionX [50]	144	15.6	0.11	-	81.1	-	✓		✓			✓				
DivaTrack [90]	16.5	3.6	0.13	22												
EgoExo4D [30]	88.8	9.6	<u>2.6</u>	<u>740</u>	<u>432</u>	<u>4405</u>		✓	✓			✓	✓	✓		
ParaHome [44]	7.33	56	4.4	30			✓		✓		✓				✓	
LaHuman [18]	3	-	0.51	-	12.3	-	✓		✓		✓	✓		✓	✓	✓
Nymeria(ours)	300	260	15	264	310.5	6545	✓	✓	✓	✓	✓	✓	✓	✓	✓	✓

**Table 2: Human motion datasets by releasing date.** Columns 2 to 5 show the recorded activity in hour (q/h), body poses in million frames (p/M), average sequence duration in minute ( $\mu$ /m) and number of participants (pp). We then compare motion with natural language annotations w.r.t. number of descriptions (nl/K) and vocabulary size (voc). The remaining columns cover the following features: using parametric human model and meshes for ground-truth motion (pm), with egocentric head-mounted device (hd), with third-person perspectives (3p), with egocentric wrist-worn device (wd), using global motion positioning (ga), with outdoor scenarios (od), with eye gaze (gz), with 3D scene representations (sr), with multi-people scenarios (mp), and human-human interactions (hh). Note EgoExo4D reports 1422h in the paper, which sums the recording hour by cameras. The total activity is 180h, with 88.8h annotated with MSCOCO keypoints. The underline numbers are reported for the full dataset.

point clouds and calibrated eye gaze – and align everything into a single, metric, world coordinate frame. In addition, XSens motion is also registered into the same reference by correcting the drift via an optimization. Overall, the dataset captured 399Km of travel by the participants for a total of 201.2M egocentric images, 11.7B IMU samples and 10.8M gaze points.

The Nymeria dataset also stands out as the world’s largest motion-language dataset. Annotators generated in-context narrations by observing the synchronized playback of rendered egocentric view, third-person view, and human motion from recorded sessions. We designed a hierarchical annotation schema to allow obtaining descriptions at different levels of detail. In total, we annotated 38.6 hours of fine-grained body poses, 207 hours with simplified atomic actions and 196 hours with activity summarization. The total descriptions contain 310.5K sentences and 8.64M words from 6545 vocabulary size.

## 2 Related Works

### 2.1 Human motion datasets

*Large-scale motion dataset.* Large-scale datasets, both real and synthetic, provide invaluable 3D annotations for analyzing movements of individuals and

groups. AMASS [58] integrates 15 mocap datasets into a unified SMPL [52] format, facilitating extensive motion analysis. 3DPW [59] employs IMUs and mobile cameras to establish the first multi-person, in-the-wild dataset with 3D keypoints. DivaTrack [90] merges synchronized body motion data and IMU signals, supporting a variety of body types and motion classes. Leveraging the GTA-V engine, GTA-Human [15] synthesizes a rich array of 3D-rendered actions, offering crucial supplements to the real data usually gathered indoors. Focusing on interaction, ParaHome [44] and HPS [34] capture human dynamics from egocentric and third-person views. ParaHome [44] records precise home activities and object movements in a unified space, whereas HPS [34] compiles an exhaustive egocentric dataset with 3D scene scans, videos, IMU data, and reconstructions of humans engaging with their surroundings, enriching the landscape of interaction perception and synthesis research.

*Egocentric multimodal motion dataset.* To advance first-person perception research, several egocentric video datasets [20–22, 29] have been developed, focusing on hand-object interaction and action recognition but often omitting 3D ground-truth data. To address this gap, datasets with comprehensive multimodal sensory data and annotations have been introduced to better capture human activities within 3D scenes. UnrealEgo [96] provides naturalistic single-person stereo images and sequences in dynamic 3D environments. EgoBody [96] is the first extensive dataset offering both egocentric and third-person views, with detailed 3D annotations for both individuals and scenes. EgoHumans [43] presents the first collection of multi-human 3D activities from egocentric perspectives. Ego-Exo4D [30], AEA [56, 57] and ADT [66] further enrich the field by documenting skilled or common daily activities.

*Motion-language dataset.* Understanding human movement semantics is enhanced by datasets with semantic labels, which vary in annotation depth. Some motion-capture (mocap) datasets [14, 28, 33, 35, 37, 80] offer sparse annotations with limited action categories, while others provide detailed semantic labels: BABEL [72] annotates AMASS [58] sequences with dense, precisely-aligned action labels via crowdsourcing. The KIT Motion-Language Dataset [71] is the first to offer complete natural language descriptions for locomotions. HumanML3D [31] enriches HumanAct12 [33] and AMASS [58] motion clips with three distinct text descriptions per clip. Motion-X [50] stands out as the first comprehensive collection of 3D whole-body motions, including facial expressions and hand gestures, with fine-grained text annotations at both sequence and frame levels.

Tab. 2 shows an overview summary. The existing human motion datasets are either captured without egocentric devices [18, 31, 44, 50, 58, 90], limited in scale [18, 34, 43, 44, 56, 66, 96], lack parametric human model for motion representation [30]. The Nymeria dataset advances the field by improving all axes.

## 2.2 Egocentric motion understanding

**Body tracking and synthesis from motion sensors.** IMU-based MoCap systems are widely adopted for capturing motion in real-world scenarios. While

tracking with fewer IMUs is much preferred in practice, it leads to ill-posed body tracking. To tackle the problems of sparsity and noise, recent methods exploit data-driven approaches to learn a motion model from large datasets. DIP [36] uses a prior based on a bi-directional RNN trained on synthesized IMU measurements from AMASS [58]. Transpose [93] further improves the tracking accuracy and addresses root translation estimation. PIP [92] adds a physics layer to refine the joint orientations and root motion predictions. TIP [41] improves root motion estimation by predicting stationary points. Some prior methods tailor tracking systems for specific off-the-shelf IMU-enabled devices, with some utilizing AR/VR devices for the head and hands [39, 40, 90], while others use mobile devices [60]. DiffusionPoser [89] takes the opposite approach by allowing the number of IMUs to be determined during inference using an inpainting technique on a pre-trained diffusion model. Alternatively, combining sparse IMUs with other egocentric modalities can enhance tracking accuracy. EgoLocate [91] combines IMUs with a monocular camera for motion tracking, device localization and mapping. MocapEveryone [46] utilizes two wrist IMUs and a head-mounted camera to capture 3D human motion in diverse environments.

**Motion synthesis from text.** Text-conditioned motion synthesis is an active research area, fueled by the availability of annotated human motion datasets such as BABEL [72] and HumanML3D [31]. Early approaches leverage variational autoencoders (VAEs) to generate diverse motions from a textual description [32, 70]. Subsequent works learn to tokenize human motion with a vector quantized variational autoencoder (VQ-VAE) to synthesize motion from text [38, 98]. MotionClip [82] also explores representation learning by training a latent space that aligns with CLIP [73] using a transformer-based autoencoder. With the advent of diffusion models, researchers have shown that higher quality and diversity in text-to-motion synthesis can be achieved with a straightforward training process [19, 79, 83]. Ongoing research refines these text-conditioned diffusion models by incorporating spatial constraints [42], generating longer motion sequences [83, 99], learning a latent space to improve generation speed and quality [17], and enhancing motion in response to fine-grained textual descriptions [94, 95]. Differing from existing human motion datasets coupled with text descriptions, the Nymeria dataset contains hierarchical language descriptions of diverse scenarios. We believe that the unprecedented diversity provided by our dataset will serve as the key ingredient for inspiring breakthroughs in the field.

### 3 Nymeria Dataset

Our goal is to record long-duration diverse daily activities with real-world settings. In addition to motion capture and headset, we also consider wristband devices, where wrist-worn sensors closely resemble current AR/VR headsets and are shown to better constrain egocentric body tracking. The remaining section details the capture setup, recording protocols, scenarios, and core statistics.



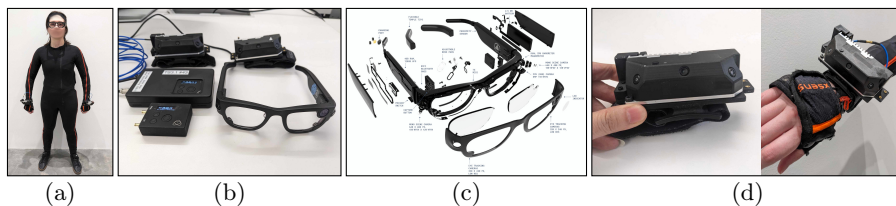


**Fig. 2: Capture setup.** From left to right: (a) a full-dressed participant who wears the mocap suit, Project Aria glasses, two miniAria wristbands and a synchronization device; (b) the set of wearble recording devices; (c) sensor suite of Project Aria and (d) miniAria wristband and how it is worn on the wrist.

### 3.1 Data capture system

**Hardware.** The capture setup is illustrated with Fig. 2. To record data, participant wears a mocap suit, a pair of Project Aria glasses, two wristbands, and a synchronization device. We use XSens MVN Link [6] for motion capture, which is a tight-fit body suit wired with 17 inertial trackers and a magnetometer. Compared to other inertial-based systems, MVN Link supports on-device recording, making it ideal for in-the-wild motion capture. To record multimodal egocentric data, we use Project Aria glasses [27] as a lightweight headset. The sensor suite includes 1 RGB camera, 2 grayscale peripheral cameras, 2 ET cameras, 2 IMUs, 1 barometer, 1 magnetometer, 7 microphones, 1 thermometer, GNSS, WiFi and BT. To resemble future wearable devices and AR/VR setup, we repackaged the electronics and sensors into a new wrist-worn device called *miniAria*. The miniAria wristband matches Project Aria glasses’s sensing ability, with exclusion of microphones, barometer, magnetometer and ET cameras. Appendix A provides further detail on sensor configuration and recording profiles.

**Synchronization.** Project Aria can record an externally provided time signal to aid synchronization. We further developed the ability for MVN Link to accept the same signal. To time align all devices, a synchronization device is developed to supply the time signal to Project Aria glasses, miniAria wristbands and mocap suit. This device can optionally receive time from a wireless server located in radio range ( $\sim 100\text{m}$ ), which enables time alignment across multiple Project Aria devices to sub-millisecond accuracy. The synchronization between mocap and Aria is within 1 motion frame *i.e.* 4.2 ms. To capture multiple people simultaneously, we replicate the described setup per participant and leverage a common time server.

### 3.2 Recording protocols

**Logistics.** We recruit diverse participants, targeting a uniform demographics among gender, age, height, and weight. During recording, an observer wearing Aria glasses is present, who is trained to participants at distance as the moving camera. This third-person holistic view provides significant extra context to

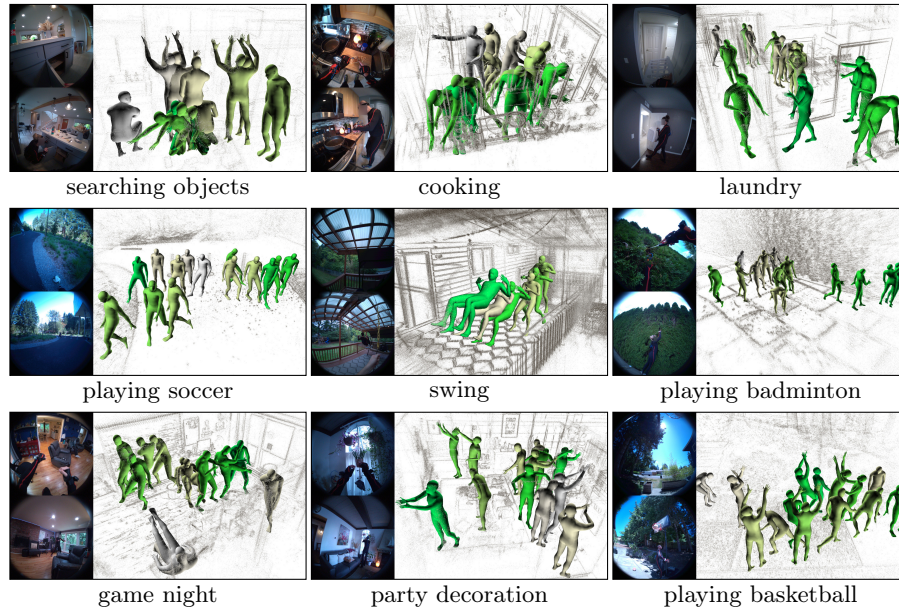


**Fig. 3: Diverse scenarios by diverse people.** We show different participants performing different indoor and outdoor activities at different locations. The top left, bottom left and right views of each subfigure shows the egocentric RGB camera view, the auxiliary third-person view and the motion, respectively.

improve motion-language narration. Besides participants and observers, two operators are onsite to manage the collection. All people interact naturally as per scenario requires, which lead to rich dynamics as opposed to staged motion. To scale collection, operators are trained to follow a 3-step procedure to complete each recording. It starts with participants performing  $<1\text{min}$  motion calibration for XSens, then  $<1\text{min}$  eye calibration for gaze estimation, and last a 15-20min activity. For one-participant collection, each person spent half a day performing 5 scenarios. For two-participant session, people are hired for a full day to collaborate on 8 scenarios. A bulk of data is captured at houses. Each location is rented for 2-4 days.

**Scenarios.** We define 20 scenarios of common daily activities (*cf.* Appendix C.1 for definitions). Typical indoor scenarios include objects searching, house touring, cooking, dining, working, entertainment etc, whereas outdoor activities include hiking, biking, sports, gardening etc. To record natural and authentic motions, we debrief participants with high-level guidelines, *e.g.* “in the following 15-20min, we will get food in the cafeteria and eat in the patio”. Most scenarios encourage human interactions, This also enables operators to prompt in-context activities to increase dynamics. Figure 1 and Fig. 3 visualize examples of the diverse scenarios.

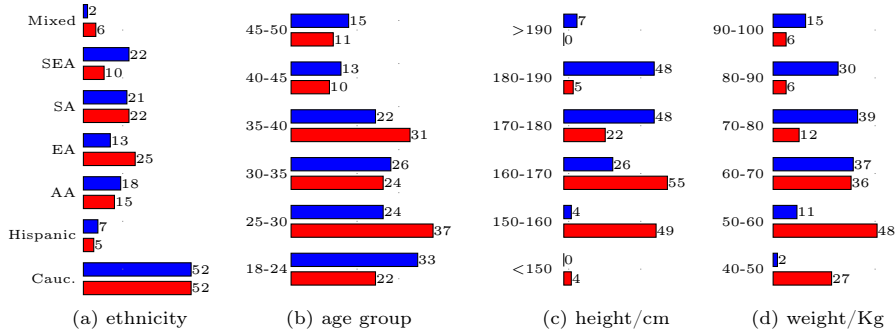


**Fig. 4: Demographics by gender.** Participants approximately split even among **female** and **male**. The ethnicity includes Caucasian (Cauc.), Hispanic, African American (AA), East Asian (EA), South Asian (SA), Southern Eastern Asian (SEA) and mixed.

### 3.3 Statistics

We collected 1200 recordings from 264 participants, which amounts to 300 hours of activities with 15min per recording on average. The accumulated trajectory from participants is 399Km for the head and 1053Km for both wrists. Collectively, we recorded 54M RGB images, 151.2M grayscale images, 11.7B IMUs samples and 10.8M gazes. Figure 4 shows the participant demographics w.r.t. the self-reported ethnicity, age, height and weight. The statistics is split by gender, where 48.5% participants self-identified as female, and 51.4% as male. The dataset captures 47 houses, where 31 are multi-floor. In total, there are 201 rooms and 45 gardens. In addition, we capture three locations from an campus, including 1 cafeteria with an outdoor patio, 1 multistory office building, and an open space with parking and multiple biking/hiking trails. Among the 1200 recordings, 228 are two-people sessions. Approximately 15% recordings contain outdoor activities. Among all scenarios, the highest occurrences are cooking, searching objects and improvised activity; whereas the lowest occurrences include working, locomotion, and creating a messy home. The statistics breakdown by scenarios and locations are detailed in Tab. 7 and Tab. 8 in Appendix C.

### 3.4 Privacy considerations

The Nymeria dataset was collected with rigorous privacy and ethics. We strictly follow Project Aria research guidelines for responsible innovation. Prior to data collection, consent was obtained from all participants and home owners regarding data recording and usage. Data was collected and stored in an anonymized way. The state-of-the-art algorithm EgoBlur [76] is used to blur faces and license plates in all videos, including data recorded at indoor closed environments. This de-identification process happened before further data processing and analysis.

## 4 Data Processing and Annotations

The data processing contains three steps. First, we use XSens software to obtain the skeleton motion, and Project Aria MPS [7] (*cf.* Appendix B.1) for device localization, scene representation and gaze estimation. Next, motion is retarget to a parametric human model and registered into the coordinates of Aria devices via optimization. Last, data is annotated with language description.

### 4.1 Full-body motion capture and retargetting

We record motion at 240Hz, following the recommended procedures: 1) carefully measuring body dimensions of participants; 2) performing calibration prior to every recording; and 3) processing with the highest XSens quality with specification of single- or multi-floor of recorded activities.

XSens represents the body motion as the global transformation and 3D local joint angles of a template skeleton. The skeleton consists of 23 segments, where each segment matches the measured body dimensions of the subject. In addition, a set of  $K = 79$  anatomical landmarks are defined on the skeleton model [62]. Their global positions,  $\{\mathbf{p}_i\}_K$ , can be computed by evaluating the forward kinematics at each frame. We utilize these landmarks to retarget the body motion onto an anatomically-inspired human model for improved realism and visual validation. Our human model is parameterized by  $\{\boldsymbol{\theta}, \boldsymbol{\phi}\}$ , where the pose parameters  $\boldsymbol{\theta}$  define the global transformation and local joint angles, and the shape parameters  $\boldsymbol{\phi}$  represent a global body scale and individual bone length. Given a motion of  $N$  frames, we solve the following inverse kinematics optimization problem:

$$\arg \min_{\boldsymbol{\phi}, \boldsymbol{\theta}_0 \dots \boldsymbol{\theta}_{T-1}, \mathbf{v}^0 \dots \mathbf{v}^{K-1}} \sum_{t=0}^{N-1} \sum_{i=0}^{K-1} \|T^i(\boldsymbol{\phi}, \boldsymbol{\theta}_t) \mathbf{v}^i - \mathbf{p}_t^i\|^2, \quad (1)$$

where  $\mathbf{v}^i$  is the local offset of the  $i$ th landmark defined on our model, and  $T^i$  is the global transformation of its parent joint. We initialize  $\mathbf{v}^i$  by manually placing them on the model. Appendix B.2 provides more details about our human model and motion retargetting.

### 4.2 6DoF localization and mapping

Data recorded at the same location are globally aligned into a single metric 3D world via Project Aria MPS [7], which employs state-of-the-art visual inertial odometry (VIO), SLAM and mapping algorithms [26, 61, 63]. In a nutshell, first SLAM is run for each individual recording independently. Subsequently, the resulting maps are loop-closed and jointly optimized via visual-inertial bundle adjustment. The output are highly accurate 1KHz trajectories as shown in Fig. 5 (*cf.* more examples with Fig. 13 in Appendix) – allowing for example to visualize head- and wrist-motion-clusters respectively.



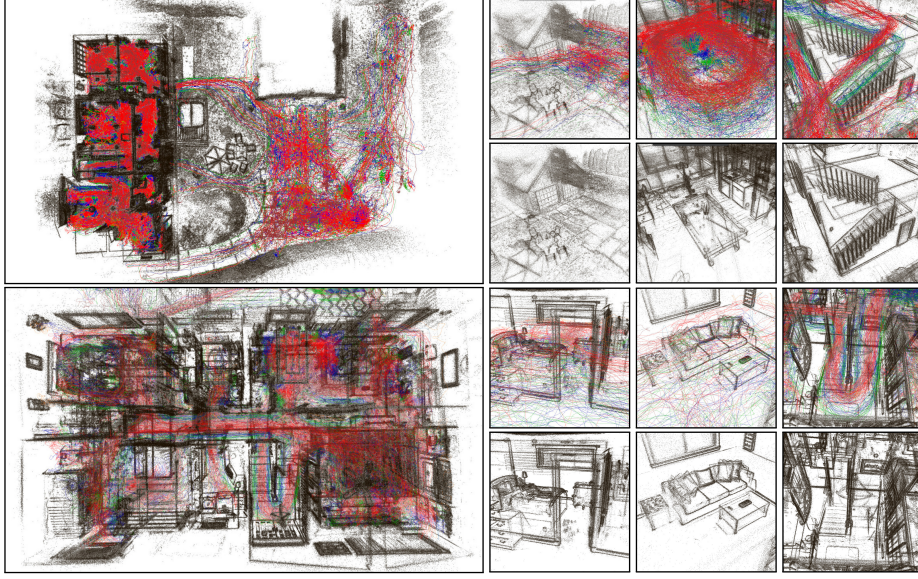


**Fig. 5: Global aligned trajectories and point clouds by locations.** We show examples of split-level residential house with gardens, where each contain  $\approx 5$  hours of recording. The left shows the top-down views of accumulated trajectories where red, green and blue indicate the head, the left and right wrist. On the right we sample closed-up views where the clusters emerge from human 3D motion distribution.

Given the device trajectories, we then align the body poses into this same frame of reference by correlating the dead-reckoned trajectory estimated by XSens. Since the latter accumulates significant drift, there exists no static global transformation to align them. Instead, we assume a constant transformation  $T_{HD}$  between the user’s head segment from XSens  $H$  and the Aria device  $D$  (Aria is firmly held in place with straps and participants are asked to avoid adjusting the glasses during the recording). We then cut the trajectory into a large number of short 4.2 ms segments, and solve the following optimization problem

$$\arg \min_{T_{HD}} \sum_t \left\| \log \left( \left( T_{OH}^t \right)^{-1} T_{OH}^{t+1} \right) \cdot \left( T_{HD} T_{WD}^t \right)^{-1} T_{WD}^{t+1} T_{HD}^{-1} \right\|^2, \quad (2)$$

where  $O$  is the drifting odometry frame of XSens and  $W$  is the world coordinates of the MPS output. This is a HandEye calibration problem with closed-form solution [81]. Note the formulation effectively aligns a large number of local motion clips by comparing the local velocity. In practice, Aria is not completely rigid during recording, resulting in a main source of inaccuracy. Precision can be improved with a rolling window optimization. Figure 6 provides a qualitative end-to-end assessment of our multi-device location, XSens motion registration, and time synchronization.

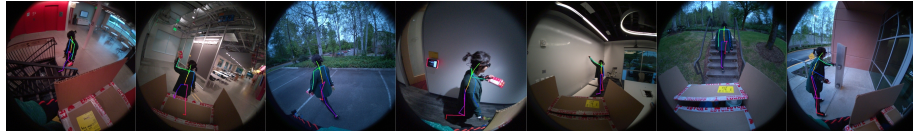


**Fig. 6: XSens skeleton projected into observer views.** We sample poses from a 20min recording spread over 1.5Km moving trajectory, and project the localized XSens skeleton into the observer RGB view for an end-to-end qualitative assessment of multi-device localization, motion registration and time synchronization. Note the subject is wearing XSens suit under a normal coat.

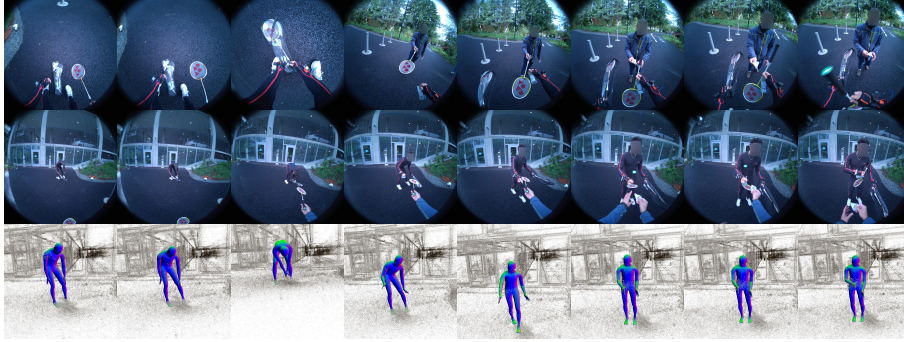
### 4.3 Language description of in-context motion

To build the connection between body motion, natural language and activity recognition, we ask human annotators to write textual descriptions of in-context human motion by viewing playback videos of the dataset. The annotators segment the video into clips to write descriptions by answering predefined questions. To give annotators a holistic understanding of the motion, the playback video contains synchronized views of the egocentric video, third-person video, and human motion rendered with 3D scene.

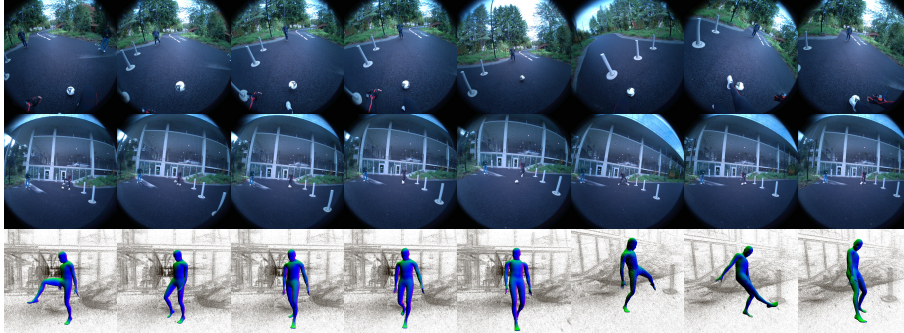
We define three annotation tasks to cover different levels of detail while scaling up human efforts in a meaningful way. The finest level is *motion narration*, with the task to describe detailed body posture, *e.g.* motion direction, velocity, how the upper body and the lower body interact with other people and the environment, the focusing attention etc. The next level annotation is *atomic action*. Compared to motion narration with elaborate descriptions, annotators are encouraged to use action verbs whenever possible, *e.g.* describing with “dancing” as opposed to “swing both arms while rotating the body to the right with legs slightly apart”. Last, we define *activity summarization*. As opposed to previous tasks which create snippets of 3-5 seconds, summarization breaks video into clips of 15-30 seconds to write one sentence summary of the high-level activity. Figure 7 provide examples of each annotation task. The figure shows the benefit of having all three synchronized views - where the egocentric view provides closed-up observations of the hand-object interactions and the environment, the third-person and motion rendering help annotators grasp a holistic understanding of the actions.

### 4.4 Data processing summary

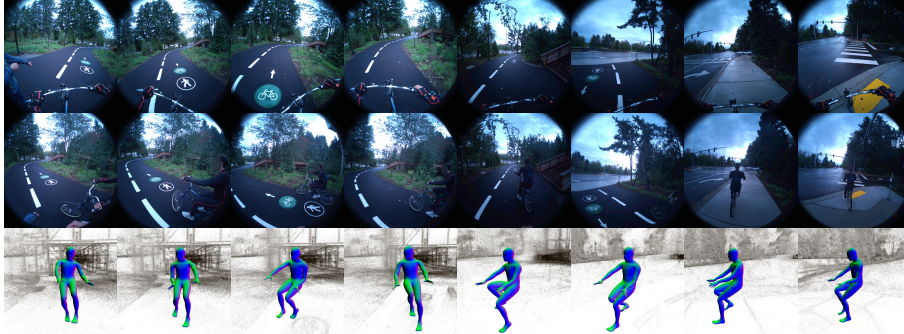
We manually inspect the XSens data to identify recordings with poor quality. We achieve 92% good-quality rate, which composes the 1200 recordings. The failure cases are mainly due to manual operational errors *e.g.* inaccurate body measurements, calibration and cable connections. We observe that MPS is highly robust with only a small fraction of recordings losing track intermittently, *i.e.* 0.38% headset and 6.3% wristband recordings. The majority of cases resume tracking shortly. Note that the fast motion and significant occlusion occurring from the



Motion narration of a 5-sec segment. “C squats to pick up the badminton bag and the soccer ball. C extends both arms straight towards the soccer ball and the badminton bag as he squats on the floor. C takes a step forward with his right foot, then bends both legs and slightly positioned both feet on tiptoe as he squats on the floor. C focuses on the soccer ball and the badminton bag.”



Atomic action of two 5-sec segments. “C lifts his right leg to prepare for a kick.” and “C kicks the soccer ball with his left feet”.



Activity summarization of a 30-sec segment. “C bikes on the road with a colleague.”

**Fig. 7: Example multi-level annotations.** From top to bottom, we show results for motion narration, atomic action and activity summarization.



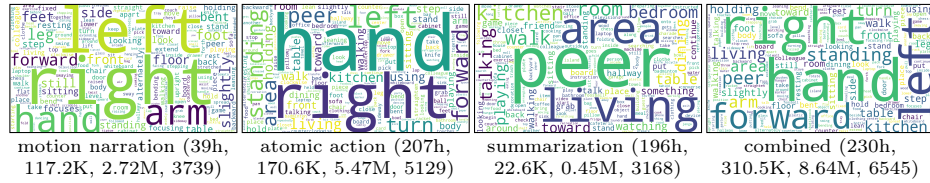


**Fig. 8: Distribution of language descriptions.** The word cloud visualizes annotations of each task in separation and with all data combined. The tuple (N, X, Y, Z) means N hours of data is described by X sentences, Y words, and Z vocabulary size.

wristband viewpoint is expected to cause a higher error rate. The breakdown statistics by scenario and location is presented in Tab. 7 and Tab. 8 in the appendix. For language descriptions, we annotated 38.6 hours motion narration, 207 hours atomic action and 196 hours activity summarization. The average video segment is 5 seconds for narration and atomic action and 30 seconds for summarization. In total, the dataset provides 310.5K sentences 8.64M words from a vocabulary of 6545 distinctive words. Note the average word per sentence is 27.8, which is significant longer than existing motion-language narrations. Figure 8 visualizes the language distribution.

## 5 Benchmark Tasks and Baselines

The large amount of diverse and contextual motion data we collected offer unprecedented opportunities in building solutions to motion tracking, synthesis, and understanding tasks, with unique multimodal egocentric sensory input and rich annotation supervisions. We present baseline results on three common problems, but they only scratch the surface of our dataset’s potential.

### 5.1 Motion generation from sparse inputs

When a user is wearing a VR headset and optionally holding controllers, or wearing a pair of AR glasses and optionally wearing wristbands, we would like to reconstruct their full body movements from onboard sensors alone. This is referred to as the "one-point" [48, 55] or "three-point" [16, 25, 40] tracking problem. Existing work can only rely on synthetic sensor input derived from motion capture datasets. Nymeria provides the first large-scale dataset of real sensor input and body motion ground truth for both model training and quantitative evaluation. It also provides real IMU data from head and wrist devices, in contrast to datasets like TotalCapture [87] or DivaTrack [90] where only IMU data from the XSens mocap system are available. As a result, future research could augment the 6D device poses with IMU and other onboard sensors [90], and/or utilize the camera views [48, 54], as well as the rich annotations in our dataset as contextual conditions for egocentric motion generation.

As baselines, we evaluate three state-of-the-art models: AvatarPoser [40] (three-point regression model), BoDiffusion [16] (three-point diffusion model),



	MPJPE			Hand	Vel.
	Mean	Lower	Upper	PE	Err.
Real	7.970	16.735	3.125	6.252	16.705
Synthetic	<b>7.309</b>	<b>15.968</b>	<b>2.508</b>	<b>3.465</b>	<b>16.633</b>

**Table 3:** The full-body three-point tracking baseline AvatarPoser [40] using the real versus synthetic input.

	MPJPE			FID
	Mean	Lower	Upper	
EgoEgo	13.216	19.032	10.002	5.14
BoDiffusion	<b>7.980</b>	<b>15.268</b>	<b>5.279</b>	<b>2.32</b>

**Table 4:** Diffusion-based motion generation baselines with one-point EgoEgo and three-point BoDiffusion.

and EgoEgo [48] (one-point diffusion model). Table 3 evaluates the reconstruction error of AvatarPoser with real and synthetic three-point input. We can see a small but noticeable quality degradation when real sensor input is used. Table 4 evaluates the two diffusion-based models additionally for their motion quality, by measuring the motion FID score [33].

## 5.2 Generative motion prior

The amount of data and the coverage in our dataset is ideal for building a foundation model of human motion. Prior attempts of learning pose [68, 84] or motion [51, 77] manifolds rely on the AMASS [58] dataset with around 40 hours of isolated motions, and with a heavy focus on locomotion or professional performance. In contrast, Nymeria consists of 300 hours of daily activities from everyday people as well as information of their surroundings when in action. Our motion distribution leads to a more suitable prior model for downstream applications that concern about everyday human activities.

Here, we provide an ablation of training a Vector-Quantized Variational Autoencoder (VQ-VAE) [24, 64] of motion data in Tab. 5 (*cf.* details in the supplementary). We compare the number of codebooks used for product quantization (PQ), codebook (CB) size, and latent dimension (Dim) against mean per-joint position error (MPJPE), Procrustes-Aligned (PA-)MPJPE, and joint position acceleration (ACC) errors. The trained encoder can be used as a "motion tokenizer" akin to a text tokenizer for language models to compress input motions as discrete codes [38], or to project noisy motion into the manifold of natural motion [77]. The resulting latent code is useful for autoregressive motion prediction in a generative motion model, with or without conditions [53]; or in a language model with text tokens for motion understanding tasks [32, 38]. When trained well, the decoder can successfully recover full motion with minimal signal loss.

## 5.3 Motion understanding in natural language

An especially valuable type of annotation in our dataset is the high quality hierarchical narrations. We provide 38.6 hours of dense motion narrations, 207 hours of atomic action and 196 hours of activity summarization in English. Compared with HumanML3D [31], our narrations are in longer natural sentences, and come with contextual descriptions of objects and environments. It can support

PQ	CB	Dim	MPJPE	PA-MPJPE	ACC
1	2048	512	51.60	37.55	1.09
2	2048	512	39.63	29.77	0.71
2	4096	512	39.20	29.66	0.82
2	16384	256	39.13	29.78	1.08
2	16384	64	<b>34.49</b>	<b>26.83</b>	<b>0.67</b>

**Table 5:** Ablation of motion VQ-VAE [mm]. Product quantization contributes the most to performance improvement, followed by increasing the codebook size while decreasing the latent dimensions.

	Bert	Bleu@1	Bleu@4	CIDEr	RougeL
TM2T	11.08	40.11	8.99	20.85	30.70
MotionGPT	<b>14.09</b>	<b>42.22</b>	<b>10.31</b>	<b>37.27</b>	<b>32.33</b>

**Table 6:** Quantitative results of motion understanding. Lacking natural language prior, TM2T performs worse than MotionGPT, which adopts T5 [75] as its language backbone. It indicates the complexity and diversity of our narration.

both texture to motion generation and motion to text description tasks, at different levels of detail. More importantly, the contextual descriptions are not only paired with the human motion, but also with videos, point clouds, and other sensory data and annotations. The corroboration of both 2D and 3D environment information with language offers exciting opportunities in grounding language and motion research in the physical world.

As baselines, we present a collection of metrics on training and testing MotionGPT [38] and TM2T [32] for the motion to text task in Tab. 6. Specifically, we report BERT score [97], BLEU score [67], CIDEr score [88] and ROUGE-L score [49]. Please refer to the supplementary for the model and training details.

## 6 Discussions and Conclusions

We propose the Nymeria dataset of unprecedented scale to accelerate the research of egocentric motion understanding. The dataset is the world’s largest collection of human motion in the wild with 300 hours daily activity, 260M body poses of 264 participants across 50 locations. We provide accurate 6DoF tracking, 3D scene representation and gaze estimation where all modalities are synchronized and aligned into a single metric coordinates. Collectively, the dataset captured 399Km of travel by the participants for a total of 201.2M egocentric images, 11.7B IMU samples and 10.8M gaze point. The Nymeria dataset also stands out as the world largest motion-language dataset with 310.5K sentences in 8.64M words text descriptions distributed in 38.6 hours of fine-grained motion narration, 207 hours atomic actions and 196 hours activity summarization.

*Limitations.* The mocap suit and miniAria wristbands lead to unnatural visual appearance which might limit the usefulness of videos for computer vision research. The setup also leads to some restriction which directly effect the range of motion. The XSens data quality is known to be affected by motion calibration and body measurements, the accuracy of which can be inconsistent across users. We are aware that our dataset only covers a portion of common daily activities. Important missing activities are the ones in public location, *e.g.* shopping

and highly dynamic motions *e.g.* driving and fast-moving sports for which our solution has limitations.

*Social impact.* Understanding egocentric full-body motion is crucial towards building contextualized AI. However the dataset and algorithms heavily involve personal data. While constructing a valuable dataset to push the boundary of technology, we make best effort respect privacy via data consent, de-identification and minimum data retention.

## References

1. Apple Vision Pro, <https://www.apple.com/apple-vision-pro/> 2
2. HTC VIVE, [vive.com](https://www.vive.com) 2
3. Magic Leap 2, <https://www.magicleap.com/magic-leap-2> 2
4. Meta Quest, <https://www.meta.com/quest/> 2
5. Microsoft HoloLens, <https://learn.microsoft.com/en-us/hololens/> 2
6. Movella XSens MVN Link motion capture, <https://www.movella.com/products/motion-capture/xsens-mvn-link> 2, 3, 7
7. Project Aria Machine Perception Services, [https://facebookresearch.github.io/projectaria\\_tools/docs/ARK/mps](https://facebookresearch.github.io/projectaria_tools/docs/ARK/mps) 3, 10, 26
8. Ray-Ban Meta smart glasses, <https://www.meta.com/smart-glasses/> 2
9. Rokoko, <https://www.rokoko.com/> 2
10. Vuzix smart glasses, <https://www.vuzix.com/pages/smart-glasses> 2
11. Akada, H., Wang, J., Shimada, S., Takahashi, M., Theobalt, C., Golyanik, V.: UnrealEgo: A new dataset for robust egocentric 3d human motion capture. In: European Conference on Computer Vision (ECCV) (2022) 2
12. Araujo, J.P., Li, J., Vetrivel, K., Agarwal, R., Gopinath, D., Wu, J., Clegg, A., Liu, C.K.: Circle: Capture in rich contextual environments. CVPR (2023) 2
13. Brown, T., Mann, B., Ryder, N., Subbiah, M., Kaplan, J.D., Dhariwal, P., Neelakantan, A., Shyam, P., Sastry, G., Askell, A., Agarwal, S., Herbert-Voss, A., Krueger, G., Henighan, T., Child, R., Ramesh, A., Ziegler, D., Wu, J., Winter, C., Hesse, C., Chen, M., Sigler, E., Litwin, M., Gray, S., Chess, B., Clark, J., Berner, C., McCandlish, S., Radford, A., Sutskever, I., Amodei, D.: Language models are few-shot learners. In: Advances in Neural Information Processing Systems. vol. 33, pp. 1877–1901 (2020) 3
14. Cai, Z., Ren, D., Zeng, A., Lin, Z., Yu, T., Wang, W., Fan, X., Gao, Y., Yu, Y., Pan, L., et al.: Humman: Multi-modal 4d human dataset for versatile sensing and modeling. In: European Conference on Computer Vision. pp. 557–577. Springer (2022) 5
15. Cai, Z., Zhang, M., Ren, J., Wei, C., Ren, D., Lin, Z., Zhao, H., Yang, L., Loy, C.C., Liu, Z.: Playing for 3d human recovery. arXiv preprint arXiv:2110.07588 (2021) 5
16. Castillo, A., Escobar, M., Jeanneret, G., Pumarola, A., Arbeláez, P., Thabet, A., Sanakoyeu, A.: BoDiffusion: Diffusing sparse observations for full-body human motion synthesis. ICCV (2023) 14, 39
17. Chen, X., Jiang, B., Liu, W., Huang, Z., Fu, B., Chen, T., Yu, G.: Executing your commands via motion diffusion in latent space. In: CVPR. pp. 18000–18010 (2023) 6
18. Cong, P., Wang, Z., Dou, Z., Ren, Y., Yin, W., Cheng, K., Sun, Y., Long, X., Zhu, X., Ma, Y.: Laserhuman: Language-guided scene-aware human motion generation in free environment (2024) 4, 5
19. Dabral, R., Mughal, M.H., Golyanik, V., Theobalt, C.: Mofusion: A framework for denoising-diffusion-based motion synthesis. In: Computer Vision and Pattern Recognition (CVPR) (2023) 6
20. Damen, D., Doughty, H., Farinella, G.M., Fidler, S., Furnari, A., Kazakos, E., Moltisanti, D., Munro, J., Perrett, T., Price, W., Wray, M.: Scaling egocentric vision: The epic-kitchens dataset. In: ECCV (2018) 5
21. Damen, D., Doughty, H., Farinella, G.M., Fidler, S., Furnari, A., Kazakos, E., Moltisanti, D., Munro, J., Perrett, T., Price, W., Wray, M.: The epic-kitchens



- dataset: Collection, challenges and baselines. *IEEE Transactions on Pattern Analysis and Machine Intelligence (TPAMI)* **43**(11), 4125–4141 (2021). <https://doi.org/10.1109/TPAMI.2020.2991965> 5
22. Damen, D., Doughty, H., Farinella, G.M., Furnari, A., Ma, J., Kazakos, E., Moltisanti, D., Munro, J., Perrett, T., Price, W., Wray, M.: Rescaling egocentric vision: Collection, pipeline and challenges for epic-kitchens-100. *IJCV* **130**, 33–55 (2022), <https://doi.org/10.1007/s11263-021-01531-2> 5
  23. Delmas, Ginger and Weinzaepfel, Philippe and Lucas, Thomas and Moreno-Noguer, Francesc and Rogez, Grégory: PoseScript: 3D Human Poses from Natural Language. In: *ECCV* (2022) 3
  24. Dhariwal, P., Jun, H., Payne, C., Kim, J.W., Radford, A., Sutskever, I.: Jukebox: A generative model for music. *arXiv preprint arXiv:2005.00341* (2020) 15, 40
  25. Du, Y., Kips, R., Pumarola, A., Starke, S., Thabet, A., Sanakoyeu, A.: Avatars grow legs: Generating smooth human motion from sparse tracking inputs with diffusion model. In: *Proceedings of the IEEE/CVF Conference on Computer Vision and Pattern Recognition*. pp. 481–490 (2023) 14
  26. Engel, J., Koltun, V., Cremers, D.: Direct sparse odometry (2016) 10
  27. Engel, J., Somasundaram, K., Goesele, M., Sun, A., Gamino, A., Turner, A., Tatlatof, A., Yuan, A., Souti, B., Meredith, B., Peng, C., Sweeney, C., Wilson, C., Barnes, D., DeTone, D., Caruso, D., Valleroy, D., Gnjupalli, D., Frost, D., Miller, E., Mueggler, E., Oleinik, E., Zhang, F., Somasundaram, G., Solaira, G., Lanaras, H., Howard-Jenkins, H., Tang, H., Kim, H.J., Rivera, J., Luo, J., Dong, J., Straub, J., Bailey, K., Eckenhoﬀ, K., Ma, L., Pesqueira, L., Schwesinger, M., Monge, M., Yang, N., Charron, N., Raina, N., Parkhi, O., Borschowa, P., Moulon, P., Gupta, P., Mur-Artal, R., Pennington, R., Kulkarni, S., Miglani, S., Gondi, S., Solanki, S., Diener, S., Cheng, S., Green, S., Saarinen, S., Patra, S., Mourikis, T., Whelan, T., Singh, T., Balntas, V., Baiyya, V., Dreewes, W., Pan, X., Lou, Y., Zhao, Y., Mansour, Y., Zou, Y., Lv, Z., Wang, Z., Yan, M., Ren, C., Nardi, R.D., Newcombe, R.: Project Aria: A new tool for egocentric multi-modal AI research (2023) 2, 3, 7, 26
  28. Ghorbani, S., Mahdavian, K., Thaler, A., Kording, K., Cook, D.J., Blohm, G., Troje, N.F.: Movi: A large multi-purpose human motion and video dataset. *Plos one* **16**(6), e0253157 (2021) 5
  29. Grauman, K., Westbury, A., Byrne, E., Chavis, Z., Furnari, A., Girdhar, R., Ham-burger, J., Jiang, H., Liu, M., Liu, X., Martin, M., Nagarajan, T., Radosavovic, I., Ramakrishnan, S.K., Ryan, F., Sharma, J., Wray, M., Xu, M., Xu, E.Z., Zhao, C., Bansal, S., Batra, D., Cartillier, V., Crane, S., Do, T., Doulaty, M., Erapalli, A., Feichtenhofer, C., Fragomeni, A., Fu, Q., Gebreselasie, A., González, C., Hillis, J., Huang, X., Huang, Y., Jia, W., Khoo, W., Kolář, J., Kottur, S., Kumar, A., Landini, F., Li, C., Li, Y., Li, Z., Mangalam, K., Modhugu, R., Munro, J., Murrell, T., Nishiyasu, T., Price, W., Ruiz, P., Ramazanova, M., Sari, L., Somasundaram, K., Southerland, A., Sugano, Y., Tao, R., Vo, M., Wang, Y., Wu, X., Yagi, T., Zhao, Z., Zhu, Y., Arbeláez, P., Crandall, D., Damen, D., Farinella, G.M., Fugen, C., Ghanem, B., Ithapu, V.K., Jawahar, C.V., Joo, H., Kitani, K., Li, H., Newcombe, R., Oliva, A., Park, H.S., Rehg, J.M., Sato, Y., Shi, J., Shou, M.Z., Torralba, A., Torresani, L., Yan, M., Malik, J.: Ego4D: Around the world in 3,000 hours of egocentric video. In: *CVPR*. pp. 18995–19012 (June 2022) 5, 32
  30. Grauman, K., Westbury, A., Torresani, L., Kitani, K., Malik, J., Afouras, T., Ashutosh, K., Baiyya, V., Bansal, S., Boote, B., Byrne, E., Chavis, Z., Chen, J., Cheng, F., Chu, F.J., Crane, S., Dasgupta, A., Dong, J., Escobar, M., Forigua,

- C., Gebreselasie, A., Haresh, S., Huang, J., Islam, M.M., Jain, S., Khirodkar, R., Kukreja, D., Liang, K.J., Liu, J.W., Majumder, S., Mao, Y., Martin, M., Mavroudi, E., Nagarajan, T., Ragusa, F., Ramakrishnan, S.K., Seminara, L., Somayazulu, A., Song, Y., Su, S., Xue, Z., Zhang, E., Zhang, J., Castillo, A., Chen, C., Fu, X., Furuta, R., Gonzalez, C., Gupta, P., Hu, J., Huang, Y., Huang, Y., Khoo, W., Kumar, A., Kuo, R., Lakhavani, S., Liu, M., Luo, M., Luo, Z., Meredith, B., Miller, A., Oguntola, O., Pan, X., Peng, P., Pramanick, S., Ramazanov, M., Ryan, F., Shan, W., Somasundaram, K., Song, C., Southerland, A., Tateno, M., Wang, H., Wang, Y., Yagi, T., Yan, M., Yang, X., Yu, Z., Zha, S.C., Zhao, C., Zhao, Z., Zhu, Z., Zhuo, J., Arbelaez, P., Bertasius, G., Crandall, D., Damen, D., Engel, J., Farinella, G.M., Furnari, A., Ghanem, B., Hoffman, J., Jawahar, C.V., Newcombe, R., Park, H.S., Rehg, J.M., Sato, Y., Savva, M., Shi, J., Shou, M.Z., Wray, M.: Ego-Exo4D: Understanding skilled human activity from first- and third-person perspectives. In: CVPR (2024) [2](#), [3](#), [4](#), [5](#)
31. Guo, C., Zou, S., Zuo, X., Wang, S., Ji, W., Li, X., Cheng, L.: Generating diverse and natural 3d human motions from text. In: Proceedings of the IEEE/CVF Conference on Computer Vision and Pattern Recognition (CVPR). pp. 5152–5161 (June 2022) [3](#), [4](#), [5](#), [6](#), [15](#)
  32. Guo, C., Zuo, X., Wang, S., Cheng, L.: Tm2t: Stochastic and tokenized modeling for the reciprocal generation of 3d human motions and texts. In: European Conference on Computer Vision. pp. 580–597. Springer (2022) [6](#), [15](#), [16](#), [40](#)
  33. Guo, C., Zuo, X., Wang, S., Zou, S., Sun, Q., Deng, A., Gong, M., Cheng, L.: Action2motion: Conditioned generation of 3d human motions. In: Proceedings of the 28th ACM International Conference on Multimedia. pp. 2021–2029 (2020) [5](#), [15](#)
  34. Guзов, V., Mir, A., Sattler, T., Pons-Moll, G.: Human pose estimation system (hps): 3d human pose estimation and self-localization in large scenes from body-mounted sensors. In: IEEE Conference on Computer Vision and Pattern Recognition (CVPR). IEEE (jun 2021) [2](#), [3](#), [4](#), [5](#)
  35. Harvey, F.G., Yurick, M., Nowrouzezahrai, D., Pal, C.: Robust motion in-betweening. ACM Transactions on Graphics (TOG) **39**(4), 60–1 (2020) [5](#)
  36. Huang, Y., Kaufmann, M., Aksan, E., Black, M.J., Hilliges, O., Pons-Moll, G.: Deep inertial poser: learning to reconstruct human pose from sparse inertial measurements in real time. ACM Transactions on Graphics (TOG) **37**(6), 1–15 (2018) [6](#)
  37. Ionescu, C., Papava, D., Olaru, V., Sminchisescu, C.: Human3. 6m: Large scale datasets and predictive methods for 3d human sensing in natural environments. IEEE transactions on pattern analysis and machine intelligence **36**(7), 1325–1339 (2013) [5](#)
  38. Jiang, B., Chen, X., Liu, W., Yu, J., Yu, G., Chen, T.: Motiongpt: Human motion as a foreign language. In: Advances in Neural Information Processing Systems (2024) [6](#), [15](#), [16](#), [40](#)
  39. Jiang, J., Streli, P., Meier, M., Fender, A., Holz, C.: Egoposer: Robust real-time ego-body pose estimation in large scenes. arXiv preprint arXiv:2308.06493 (2023) [6](#)
  40. Jiang, J., Streli, P., Qiu, H., Fender, A., Laich, L., Snape, P., Holz, C.: Avatarposer: Articulated full-body pose tracking from sparse motion sensing. In: European Conference on Computer Vision. pp. 443–460. Springer (2022) [2](#), [6](#), [14](#), [15](#), [39](#)
  41. Jiang, Y., Ye, Y., Gopinath, D., Won, J., Winkler, A.W., Liu, C.K.: Transformer inertial poser: Real-time human motion reconstruction from sparse imu with simul-

- taneous terrain generation. In: SIGGRAPH Asia 2022 Conference Papers. pp. 1–9 (2022) [2](#), [6](#)
42. Karunratanakul, K., Preechakul, K., Suwajanakorn, S., Tang, S.: Guided motion diffusion for controllable human motion synthesis. In: Proceedings of the IEEE/CVF International Conference on Computer Vision. pp. 2151–2162 (2023) [6](#)
  43. Khirodkar, R., Bansal, A., Ma, L., Newcombe, R., Vo, M., Kitani, K.: EgoHumans: An egocentric 3d multi-human benchmark. In: ICCV (2023) [2](#), [3](#), [4](#), [5](#)
  44. Kim, J., Kim, J., Na, J., Joo, H.: Parahome: Parameterizing everyday home activities towards 3d generative modeling of human-object interactions (2024) [2](#), [4](#), [5](#)
  45. Lee, J., Joo, H.: Locomotion-action-manipulation: Synthesizing human-scene interactions in complex 3d environments. ICCV (2023) [2](#)
  46. Lee, J., Joo, H.: Mocap everyone everywhere: Lightweight motion capture with smartwatches and a head-mounted camera. arXiv preprint arXiv:2401.00847 (2024) [2](#), [6](#)
  47. Li, G., Zhao, K., Zhang, S., Lyu, X., Dusmanu, M., Zhang, Y., Pollefeys, M., Tang, S.: Egogen: An egocentric synthetic data generator (2024) [2](#)
  48. Li, J., Liu, K., Wu, J.: Ego-body pose estimation via ego-head pose estimation. In: Proceedings of the IEEE/CVF Conference on Computer Vision and Pattern Recognition. pp. 17142–17151 (2023) [14](#), [15](#), [39](#)
  49. Lin, C.Y.: Rouge: A package for automatic evaluation of summaries. In: Text summarization branches out. pp. 74–81 (2004) [16](#)
  50. Lin, J., Zeng, A., Lu, S., Cai, Y., Zhang, R., Wang, H., Zhang, L.: Motion-x: A large-scale 3d expressive whole-body human motion dataset. Advances in Neural Information Processing Systems (2023) [2](#), [4](#), [5](#)
  51. Ling, H.Y., Zinno, F., Cheng, G., van de Panne, M.: Character controllers using motion vaes. ACM Trans. Graph. **39**(4) (2020) [15](#)
  52. Loper, M., Mahmood, N., Romero, J., Pons-Moll, G., Black, M.J.: SMPL: A skinned multi-person linear model. ACM Trans. Graphics (Proc. SIGGRAPH Asia) **34**(6), 248:1–248:16 (Oct 2015) [5](#), [39](#)
  53. Lucas, T., Baradel, F., Weinzaepfel, P., Rogez, G.: Posegpt: Quantization-based 3d human motion generation and forecasting. In: European Conference on Computer Vision. pp. 417–435. Springer (2022) [15](#), [40](#)
  54. Luo, Z., Cao, J., Khirodkar, R., Winkler, A., Kitani, K., Xu, W.: Real-time simulated avatar from head-mounted sensors. In: Proceedings IEEE/CVF Conf. on Computer Vision and Pattern Recognition (CVPR) (2024) [14](#)
  55. Luo, Z., Hachiuma, R., Yuan, Y., Kitani, K.: Dynamics-regulated kinematic policy for egocentric pose estimation. In: Neural Information Processing Systems (2021) [14](#)
  56. Lv, Z., Charron, N., Moulon, P., Gamino, A., Peng, C., Sweeney, C., Miller, E., Tang, H., Meissner, J., Dong, J., et al.: Aria everyday activities dataset. arXiv preprint arXiv:2402.13349 (2024) [5](#)
  57. Lv, Z., Miller, E., Meissner, J., Pesqueira, L., Sweeney, C., Dong, J., Ma, L., Patel, P., Moulon, P., Somasundaram, K., Parkhi, O., Zou, Y., Raina, N., Saarinen, S., Mansour, Y.M., Huang, P.K., Wang, Z., Troynikov, A., Artal, R.M., DeTone, D., Barnes, D., Argall, E., Lobanovskiy, A., Kim, D.J., Bouttefroy, P., Straub, J., Engel, J.J., Gupta, P., Yan, M., Nardi, R.D., Newcombe, R.: Aria pilot dataset. <https://about.facebook.com/realitylabs/projectaria/datasets> (2022) [5](#)

58. Mahmood, N., Ghorbani, N., Troje, N.F., Pons-Moll, G., Black, M.J.: AMASS: Archive of motion capture as surface shapes. In: International Conference on Computer Vision. pp. 5442–5451 (Oct 2019) [2](#), [4](#), [5](#), [6](#), [15](#)
59. von Marcard, T., Henschel, R., Black, M.J., Rosenhahn, B., Pons-Moll, G.: Recovering accurate 3d human pose in the wild using imus and a moving camera. In: Proceedings of the European Conference on Computer Vision (ECCV) (September 2018) [2](#), [5](#)
60. Mollyn, V., Arakawa, R., Goel, M., Harrison, C., Ahuja, K.: Imuposer: Full-body pose estimation using imus in phones, watches, and earbuds. In: Proceedings of the 2023 CHI Conference on Human Factors in Computing Systems. CHI '23, Association for Computing Machinery, New York, NY, USA (2023). <https://doi.org/10.1145/3544548.3581392>, <https://doi.org/10.1145/3544548.3581392> [6](#)
61. Mourikis, A.I., Roumeliotis, S.I.: A multi-state constraint kalman filter for vision-aided inertial navigation. In: Proceedings 2007 IEEE international conference on robotics and automation. pp. 3565–3572. IEEE (2007) [10](#)
62. Movella: MVN User Manual, [https://www.movella.com/hubfs/MVN\\_User\\_Manual.pdf](https://www.movella.com/hubfs/MVN_User_Manual.pdf) [10](#), [31](#)
63. Mur-Artal, R., Montiel, J.M.M., Tardós, J.D.: ORB-SLAM: a versatile and accurate monocular SLAM system. IEEE Transactions on Robotics **31**(5), 1147–1163 (2015). <https://doi.org/10.1109/TRO.2015.2463671> [10](#)
64. van den Oord, A., Vinyals, O., Kavukcuoglu, K.: Neural discrete representation learning. In: Proceedings of the 31st International Conference on Neural Information Processing Systems (2017) [15](#), [40](#)
65. OpenAI, :, Achiam, J., Adler, S., Agarwal, S., Ahmad, L., Akkaya, I., Aleman, F.L., Almeida, D., Altenschmidt, J., Altman, S., Anadkat, S., Avila, R., Babuschkin, I., Balaji, S., Balcom, V., Baltescu, P., Bao, H., Bavarian, M., Belgum, J., Bello, I., Berdine, J., Bernadett-Shapiro, G., Berner, C., Bogdonoff, L., Boiko, O., Boyd, M., Brakman, A.L., Brockman, G., Brooks, T., Brundage, M., Button, K., Cai, T., Campbell, R., Cann, A., Carey, B., Carlson, C., Carmichael, R., Chan, B., Chang, C., Chantzis, F., Chen, D., Chen, S., Chen, R., Chen, J., Chen, M., Chess, B., Cho, C., Chu, C., Chung, H.W., Cummings, D., Currier, J., Dai, Y., Decareaux, C., Degry, T., Deutsch, N., Deville, D., Dhar, A., Dohan, D., Dowling, S., Dunning, S., Ecoffet, A., Eleti, A., Eloundou, T., Farhi, D., Fedus, L., Felix, N., Fishman, S.P., Forte, J., Fulford, I., Gao, L., Georges, E., Gibson, C., Goel, V., Gogineni, T., Goh, G., Gontijo-Lopes, R., Gordon, J., Grafstein, M., Gray, S., Greene, R., Gross, J., Gu, S.S., Guo, Y., Hallacy, C., Han, J., Harris, J., He, Y., Heaton, M., Heidecke, J., Hesse, C., Hickey, A., Hickey, W., Hoeschele, P., Houghton, B., Hsu, K., Hu, S., Hu, X., Huizinga, J., Jain, S., Jain, S., Jang, J., Jiang, A., Jiang, R., Jin, H., Jin, D., Jomoto, S., Jonn, B., Jun, H., Kaftan, T., Łukasz Kaiser, Kamali, A., Kanitscheider, I., Keskar, N.S., Khan, T., Kilpatrick, L., Kim, J.W., Kim, C., Kim, Y., Kirchner, H., Kiros, J., Knight, M., Kokotajlo, D., Łukasz Kondraciuk, Kondrich, A., Konstantinidis, A., Kosic, K., Krueger, G., Kuo, V., Lampe, M., Lan, I., Lee, T., Leike, J., Leung, J., Levy, D., Li, C.M., Lim, R., Lin, M., Lin, S., Litwin, M., Lopez, T., Lowe, R., Lue, P., Makanju, A., Malfacini, K., Manning, S., Markov, T., Markovski, Y., Martin, B., Mayer, K., Mayne, A., McGrew, B., McKinney, S.M., McLeavey, C., McMillan, P., McNeil, J., Medina, D., Mehta, A., Menick, J., Metz, L., Mishchenko, A., Mishkin, P., Monaco, V., Morikawa, E., Mossing, D., Mu, T., Murati, M., Murk, O., Mély, D., Nair, A., Nakano, R., Nayak, R., Neelakantan, A., Ngo, R., Noh, H., Ouyang, L., O’Keefe, C., Pachocki, J., Paino, A., Palermo, J., Pantuliano, A., Parascandolo, G., Parish, J., Parparita, E., Passos, A., Pavlov, M.,

- Peng, A., Perelman, A., de Avila Belbute Peres, F., Petrov, M., de Oliveira Pinto, H.P., Michael, Pokorny, Pokrass, M., Pong, V., Powell, T., Power, A., Power, B., Proehl, E., Puri, R., Radford, A., Rae, J., Ramesh, A., Raymond, C., Real, F., Rimbach, K., Ross, C., Rotsted, B., Roussez, H., Ryder, N., Saltarelli, M., Sanders, T., Santurkar, S., Sastry, G., Schmidt, H., Schnurr, D., Schulman, J., Selsam, D., Sheppard, K., Sherbakov, T., Shieh, J., Shoker, S., Shyam, P., Sidor, S., Sigler, E., Simens, M., Sitkin, J., Slama, K., Sohl, I., Sokolowsky, B., Song, Y., Staudacher, N., Such, F.P., Summers, N., Sutskever, I., Tang, J., Tezak, N., Thompson, M., Tillet, P., Tootoonchian, A., Tseng, E., Tuggle, P., Turley, N., Tworek, J., Uribe, J.F.C., Vallone, A., Vijayvergiya, A., Voss, C., Wainwright, C., Wang, J.J., Wang, A., Wang, B., Ward, J., Wei, J., Weinmann, C., Welihinda, A., Welinder, P., Weng, J., Weng, L., Wiethoff, M., Willner, D., Winter, C., Wolrich, S., Wong, H., Workman, L., Wu, S., Wu, J., Wu, M., Xiao, K., Xu, T., Yoo, S., Yu, K., Yuan, Q., Zaremba, W., Zellers, R., Zhang, C., Zhang, M., Zhao, S., Zheng, T., Zhuang, J., Zhuk, W., Zoph, B.: Gpt-4 technical report (2023) **3**
66. Pan, X., Charron, N., Yang, Y., Peters, S., Whelan, T., Kong, C., Parkhi, O., Newcombe, R., Ren, C.Y.: Aria digital twin: A new benchmark dataset for egocentric 3d machine perception (2023) **2, 5**
  67. Papineni, K., Roukos, S., Ward, T., Zhu, W.J.: Bleu: a method for automatic evaluation of machine translation. In: Proceedings of the 40th annual meeting of the Association for Computational Linguistics. pp. 311–318 (2002) **16**
  68. Pavlakos, G., Choutas, V., Ghorbani, N., Bolkart, T., Osman, A.A.A., Tzionas, D., Black, M.J.: Expressive body capture: 3D hands, face, and body from a single image. In: Proceedings IEEE Conf. on Computer Vision and Pattern Recognition (CVPR). pp. 10975–10985 (2019) **15**
  69. Peebles, W., Xie, S.: Scalable diffusion models with transformers. In: Proceedings of the IEEE/CVF International Conference on Computer Vision. pp. 4195–4205 (2023) **39**
  70. Petrovich, M., Black, M.J., Varol, G.: Temos: Generating diverse human motions from textual descriptions. In: ECCV. pp. 480–497. Springer Nature Switzerland, Cham (2022) **6**
  71. Plappert, M., Mandery, C., Asfour, T.: The KIT motion-language dataset. Big Data **4**(4), 236–252 (dec 2016). <https://doi.org/10.1089/big.2016.0028>, <http://dx.doi.org/10.1089/big.2016.0028> **3, 5**
  72. Punnaakkal, A.R., Chandrasekaran, A., Athanasiou, N., Quiros-Ramirez, A., Black, M.J.: BABEL: Bodies, action and behavior with english labels. In: Proceedings IEEE/CVF Conf. on Computer Vision and Pattern Recognition (CVPR). pp. 722–731 (Jun 2021) **5, 6**
  73. Radford, A., Kim, J.W., Hallacy, C., Ramesh, A., Goh, G., Agarwal, S., Sastry, G., Askell, A., Mishkin, P., Clark, J., Krueger, G., Sutskever, I.: Learning transferable visual models from natural language supervision (2021) **6**
  74. Radford, A., Wu, J., Child, R., Luan, D., Amodei, D., Sutskever, I.: Language models are unsupervised multitask learners (2019) **40**
  75. Raffel, C., Shazeer, N., Roberts, A., Lee, K., Narang, S., Matena, M., Zhou, Y., Li, W., Liu, P.J.: Exploring the limits of transfer learning with a unified text-to-text transformer. The Journal of Machine Learning Research **21**(1), 5485–5551 (2020) **16, 40**
  76. Raina, N., Somasundaram, G., Zheng, K., Saarinen, S., Messiner, J., Schwesinger, M., Pesqueira, L., Prasad, I., Miller, E., Gupta, P., Yan, M., Newcombe, R.A., Ren, C.Y., Parkhi, O.M.: Egoblur: Responsible innovation in aria.

- ArXiv **abs/2308.13093** (2023), <https://api.semanticscholar.org/CorpusID:261214435> **9**
77. Rempe, D., Birdal, T., Hertzmann, A., Yang, J., Sridhar, S., Guibas, L.J.: Humor: 3d human motion model for robust pose estimation. In: International Conference on Computer Vision (ICCV) (2021) **15**
  78. Roetenberg, D., Luinge, H., Slycke, P.: Xsens mvn: Full 6dof human motion tracking using miniature inertial sensors. Xsens Motion Technol. BV Tech. Rep. **3** (01 2009) **2**
  79. Shafir, Y., Tevet, G., Kapon, R., Bermano, A.H.: Human motion diffusion as a generative prior. ICLR (2023) **6**
  80. Shahroudy, A., Liu, J., Ng, T.T., Wang, G.: Ntu rgb+ d: A large scale dataset for 3d human activity analysis. In: Proceedings of the IEEE conference on computer vision and pattern recognition. pp. 1010–1019 (2016) **5**
  81. Sorkine-Hornung, O., Rabinovich, M.: Least-squares rigid motion using svd. Computing **1**(1), 1–5 (2017) **11**
  82. Tevet, G., Gordon, B., Hertz, A., Bermano, A.H., Cohen-Or, D.: Motionclip: Exposing human motion generation to clip space. In: Computer Vision–ECCV 2022: 17th European Conference, Tel Aviv, Israel, October 23–27, 2022, Proceedings, Part XXII. pp. 358–374. Springer (2022) **6**
  83. Tevet, G., Raab, S., Gordon, B., Shafir, Y., Cohen-or, D., Bermano, A.H.: Human motion diffusion model. In: ICLR (2023) **6**
  84. Tiwari, G., Antic, D., Lenssen, J.E., Sarafianos, N., Tung, T., Pons-Moll, G.: Pose-ndf: Modeling human pose manifolds with neural distance fields. In: European Conference on Computer Vision (ECCV) (October 2022) **15**
  85. Tome, D., Alldieck, T., Peluse, P., Pons-Moll, G., Agapito, L., Badino, H., de la Torre, F.: Selfpose: 3d egocentric pose estimation from a headset mounted camera. IEEE Transactions on Pattern Analysis and Machine Intelligence (Oct 2020) **2**
  86. Touvron, H., Lavril, T., Izacard, G., Martinet, X., Lachaux, M.A., Lacroix, T., Rozière, B., Goyal, N., Hambro, E., Azhar, F., Rodriguez, A., Joulin, A., Grave, E., Lample, G.: Llama: Open and efficient foundation language models (2023) **3**
  87. Trumble, M., Gilbert, A., Malleson, C., Hilton, A., Collomosse, J.: Total capture: 3d human pose estimation fusing video and inertial sensors. In: Proceedings of 28th British Machine Vision Conference. pp. 1–13 (2017) **14**
  88. Vedantam, R., Lawrence Zitnick, C., Parikh, D.: Cider: Consensus-based image description evaluation. In: Proceedings of the IEEE conference on computer vision and pattern recognition. pp. 4566–4575 (2015) **16**
  89. Wouwe, T., Lee, S., Falisse, A., Delp, S., Liu, C.: Diffusion inertial poser: Human motion reconstruction from arbitrary sparse imu configurations. In: CVPR (2024) **6**
  90. Yang, D., Kang, J., Ma, L., Greer, J., Ye, Y., Lee, S.H.: Divatrack: Diverse bodies and motions from acceleration-enhanced three-point trackers. EuroGraphics (2024) **2, 4, 5, 6, 14**
  91. Yi, X., Zhou, Y., Habermann, M., Golyanik, V., Pan, S., Theobalt, C., Xu, F.: EgoLocate: Real-time motion capture, localization, and mapping with sparse body-mounted sensors. ACM Transactions on Graphics (TOG) **42**(4) (2023) **6**
  92. Yi, X., Zhou, Y., Habermann, M., Shimada, S., Golyanik, V., Theobalt, C., Xu, F.: Physical inertial poser (pip): Physics-aware real-time human motion tracking from sparse inertial sensors. In: Proceedings of the IEEE/CVF Conference on Computer Vision and Pattern Recognition. pp. 13167–13178 (2022) **6**

93. Yi, X., Zhou, Y., Xu, F.: Transpose: real-time 3d human translation and pose estimation with six inertial sensors. *ACM Transactions on Graphics (TOG)* **40**(4), 1–13 (2021) [6](#)
94. Zhang, M., Cai, Z., Pan, L., Hong, F., Guo, X., Yang, L., Liu, Z.: Motiondiffuse: Text-driven human motion generation with diffusion model. *arXiv preprint arXiv:2208.15001* (2022) [6](#)
95. Zhang, M., Li, H., Cai, Z., Ren, J., Yang, L., Liu, Z.: Finemogen: Fine-grained spatio-temporal motion generation and editing. *NeurIPS* (2023) [6](#)
96. Zhang, S., Ma, Q., Zhang, Y., Qian, Z., Kwon, T., Pollefeys, M., Bogo, F., Tang, S.: EgoBody: Human body shape and motion of interacting people from head-mounted devices. In: *European conference on computer vision (ECCV)* (Oct 2022) [2](#), [3](#), [4](#), [5](#)
97. Zhang, T., Kishore, V., Wu, F., Weinberger, K.Q., Artzi, Y.: Bertscore: Evaluating text generation with bert. *arXiv preprint arXiv:1904.09675* (2019) [16](#)
98. Zhang, Y., Huang, D., Liu, B., Tang, S., Lu, Y., Chen, L., Bai, L., Chu, Q., Yu, N., Ouyang, W.: Motiongpt: Finetuned llms are general-purpose motion generators. *arXiv preprint arXiv:2306.10900* (2023) [6](#), [40](#)
99. Zhang, Z., Liu, R., Aberman, K., Hanocka, R.: Tedi: Temporally-entangled diffusion for long-term motion synthesis (2023) [6](#)



## Appendix

The appendix provides further details about the dataset and algorithms. The structure is as follows. Appendix A gives more details about the capture setup. Appendix B provides descriptions about data processing, including a brief summary of Project Aria MPS [7] in Appendix B.1, XSens motion retargetting in Appendix B.2, and motion-language narration interface in Appendix B.3. Appendix C provides additional oversights of dataset construction w.r.t. recording scenarios (Appendix C.1) and locations (Appendix C.2). Appendix D discusses details about the baseline experiments. Appendix E presents the contribution statement and acknowledgement.

### A Hardware

Figure 9 compares camera viewpoints of Project Aria glasses and miniAria wristbands for 4 common body postures. The sensor suite of Project Aria is detailed in [27]. The miniAria wristbands uses almost identical electronics and sensors, with the exclusion of microphones, barometer, magnetometer and ET cameras. The dynamic range of IMUs on miniAria is increased to count for fast wrist motion. For Project Aria, the left IMU accelerometer saturates at 4g and gyroscope at  $500^\circ/\text{s}$ , and the right IMU accelerometer saturates at 8g and gyroscope at  $1000^\circ/\text{s}$ . The saturation range is doubled for both IMUs on miniAria accordingly.

**Recording profile.** Project Aria glasses is set to record 30fps RGB video at  $1408 \times 1408$  pixel resolution, 30fps grayscale videos at  $640 \times 480$  pixel resolution, 10fps eye tracking videos at  $320 \times 240$  pixel resolution, 1KHz IMU measurements for the right IMU, 800Hz IMU measurements for the left IMU, 10Hz magnetometer measurements, 50Hz barometer measurements, and 48KHz 7-channel audio. The GNSS, WiFi and BT are turned off for privacy consideration. Similarly, miniAria wristbands record 10fps RGB video at  $1408 \times 1408$  pixel resolution, 20fps grayscale videos at  $640 \times 480$  pixel resolution, 1KHz and 800Hz IMU measurements for the right and left IMU respectively. miniAria does not have audio, magnetometer and barometer sensors. The XSens Analyse Pro records 1KHz IMUs and outputs 240Hz full-body motion.

### B Data Processing

#### B.1 Project Aria MPS

Project Aria’s machine perception service (MPS) provides building-block algorithms to simplify the processing of the different sensor streams. These functionalities are likely to be available to run on device in real-time for future AR- or smart-glasses. We use the following core functionalities currently offered by Project Aria, and include their raw output as part of the dataset. See [27] and the technical documentation<sup>5</sup> for more details.

<sup>5</sup> [https://facebookresearch.github.io/projectaria\\_tools/docs/data\\_formats](https://facebookresearch.github.io/projectaria_tools/docs/data_formats)

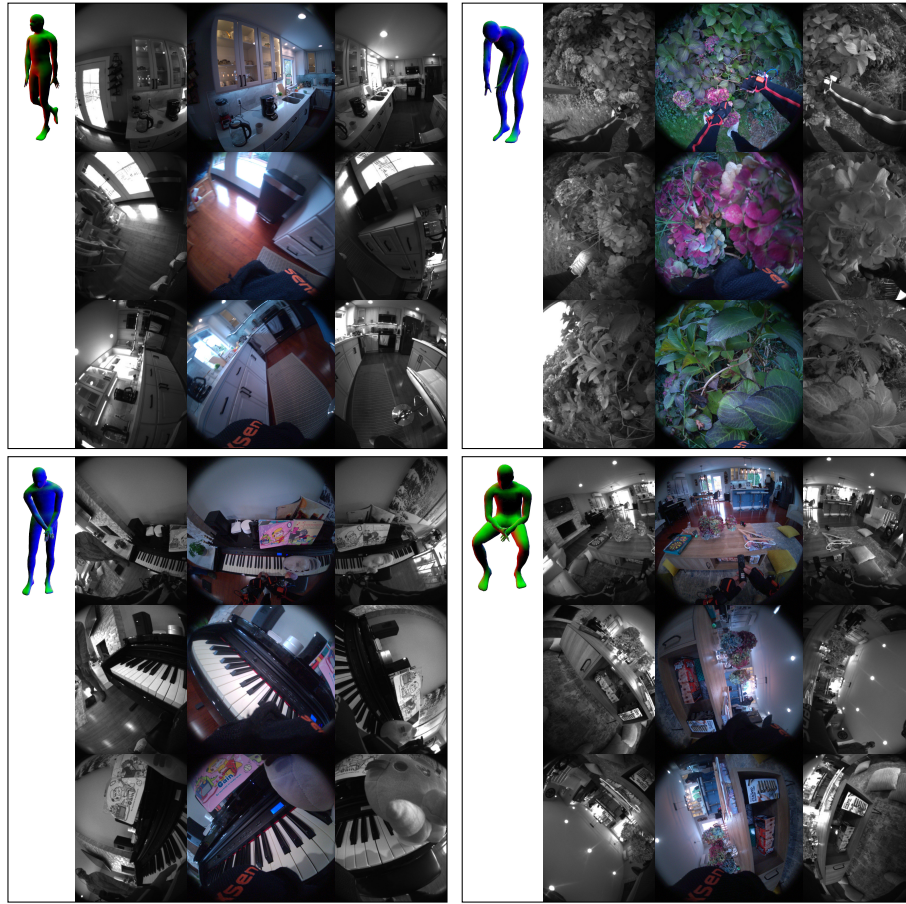


**Fig. 9: Viewpoints comparison of common body poses.** In each sub-figure, we show the left grayscale camera, RGB camera, the right grayscale camera of Aria glasses (top), left miniAria wristband (middle) and the right miniAria wristband (bottom), respectively.

*Calibration.* All Aria and miniAria sensors are intrinsically and extrinsically calibrated. For cameras, we use a spherical (equidistant) base model, with additional coefficients for radial, tangential, and thin-prism distortion. Besides this fixed per-device factory calibration, MPS computes time-varying online-calibration as part of the output, that corrects for tiny deformations due to temperature changes or stress applied to the glasses frame.

*The 6DoF localization.* Every recording is localized precisely and robustly in a common, metric, gravity-aligned coordinate frame, using a state-of-the-art visual inertial odometry (VIO) and simultaneous localization and mapping (SLAM) algorithms. This provides millimeter-accurate 6DoF poses for every captured frame and 1 KHz high-frequency motion in-between camera frames. We provide both a *closed-loop trajectory* that is aligned to this common coordinate frame, as well as the *open-loop trajectory* that is the result of VIO dead-reckoning by strictly causal computing.

*Eye gaze.* The gaze direction of the user is estimated as a two outward-facing rays, anchored on the left and right eye respectively. This allows to compute both the direction in which the wearer is looking, as well as – approximately – the metric distance at which they are focusing their eyes. We use an optional eye gaze calibration procedure, where the mobile companion app directs the wearer to gaze at a pattern on the phone screen while performing specific head movements. This information was then used to generate a more accurate eye gaze direction, personalized to the particular wearer.

*Point cloud maps.* The 3D point cloud of temporary static scene elements is triangulated from the moving Aria device, using the photometric stereo over consecutive frames and across the left and right monochrome cameras. The output contains the triangulated 3D point clouds, as well as the raw, causally computed, 2D observations of every point in the monochrome camera. The latter allows to compute when each triangulated point is observed – which can be important to account for, when objects of furniture is moved within scripts.

## B.2 Motion retargeting

Here we present details on the human model used to represent the ground truth body motion, and the optimization solver for motion retargeting from XSens output. Examples of retargeting results are shown in Fig. 11. We will release the model and the solver library upon dataset release.

*Human model.* Our human model showing in Fig. 10 (left) consists of 159 skeletal joints that deform a manifold quadrangle mesh through linear blend skinning (LBS). Among them, 28 joints control the face, such as eyes, jaw, and the tongue; and 42 joints control all fingers on both hands, 21 joints on each side. The remaining 89 joints that control the body are what we use in retargeting to

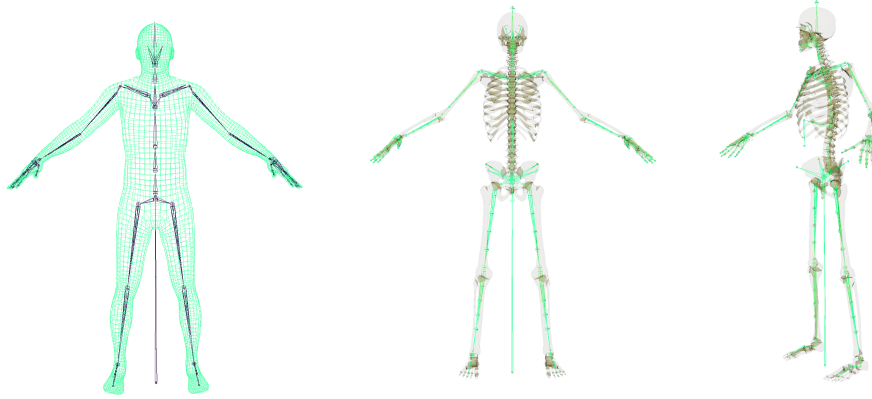


**Fig. 10: Our anatomically inspired human model.** Its joints are designed and placed to follow human anatomy. Left: frontal view of the skeleton (dark) and the body quadmesh (green). Middle: frontal view of the skeleton overlay on a skeleton model. Right: side view of the skeleton model.

represent the body motion ground truth, while leaving the face and finger joints unchanged.

Among the 89 body joints, we use one joint to represent the global transformation in the world. 35 joints are designed to represent bones in the human body and they loosely follow the human anatomical structure (*e.g.* the forearm joint corresponds to the ulna and serves as the twist pivot of the wrist, which is located at the tip of what would be the radius). Fig. 10 (middle, right) overlays the joints on a skeleton model for reference. In addition, we designed 53 "helper" joints for the purpose of improving skinning deformation, as commonly done in computer graphics. These helper joints are driven by the 35 bones with a simple linear relationship. For example, there are five helper joints along each upper and lower limb respectively. Their purpose is to distribute the twist rotation values between the two end joints along the limbs, to avoid the "candy wrapper" artifact of linear blend skinning.

*Model parameterization.* The body model is parameterized by identity parameters  $\phi \in \mathbf{R}^{12}$  and pose parameters  $\theta \in \mathbf{R}^{58}$ . They are designed manually from heuristics to follow anatomical principles while reducing mode complexity. The identity parameters consist of a global scale of the model, three end effector scales (*i.e.* hand, hands, and feet), and eight translations that represent bone lengths symmetrically for both sides (*i.e.* hip width, spine length, neck length, shoulder width, upper arm length, lower arm length, upper leg length, lower leg length). The translation values offset the position of a joint in its local space (*i.e.* parent space). The 58 pose parameters consist of 6 DoF for the global transformation, and 52 euler angles that represent local joint rotations. This is a reduced set of rotations for the 35 joints since we model limits and synergies of joints. For

example, the elbows and knees only have one rotational DoF. And we control the four spine joints with only two groups of 3D rotations, which co-activate adjacent spine joints with a fall off for better postures. The specific definitions of these parameters will be released with the model.

Since XSens provides only skeletal poses with no body shape information, we do not change the body mesh from the template for an individual, except for skinning deformations from the identity parameters.

*Optimization solver.* As described in the paper, we solve an inverse kinematics optimization problem using anatomical landmarks from XSens. We manually define the location of these landmarks on our human model and parent them rigidly under appropriate joints. We don’t expect our manual definition to be accurate, so we only use them as an initial guess, and aim to solve the local landmark locations in the optimization. For every motion, XSens outputs the global locations of these landmarks, which we take as input, and solve for the identity parameters of the user, the landmark offsets, and the per-frame pose parameters using Equation (1). This non-linear least-square optimization is solved using the Levenberg–Marquardt algorithm.

The data from XSens often contain various artifacts. Two main sources of error are inaccurate body dimension measurements, and the simplified skeleton model XSens uses to solve for body motions from their sensor measurements. They result in body self-penetrations, especially between the hands and the body, and unnatural poses. To mitigate these artifacts, we incorporate two additional loss terms as the optimization objective: parameter limits and body collisions penalty. Parameter limits are defined as quadratic falloffs at the manually designed boundaries. Body collisions are computed from manually defined collision proxies (*i.e.* tapered capsules) for each body part. At every optimization step, we compute pairs of colliding bodies, and penalize the penetration distance. Optionally, we can also use a smoothness objective to penalize change of pose parameters between consecutive frames. Because these objectives are also expressed as least-square functions, they can be optimized using the Levenberg–Marquardt algorithm as well.

In practice, a motion sequence can be several minutes long and it is difficult and expensive to solve the entire sequence all together. We instead solve Equation (1) from only a subset of uniformly sampled frames (*e.g.* 200 frames) from a long sequence to obtain the identity parameters and landmark offsets. We then use them to solve for pose parameters for the entire sequence frame-by-frame, which is much simpler and faster.

### B.3 In-context motion narration

We employ 25 annotators to write text descriptions in English for the dataset. Compare to the existing motion-language narration, our goal is to obtain in-context annotations that aligns full-body motion, egocentric perception, and language by offering descriptions about body poses and how the wearers interact with objects, environments and other people.

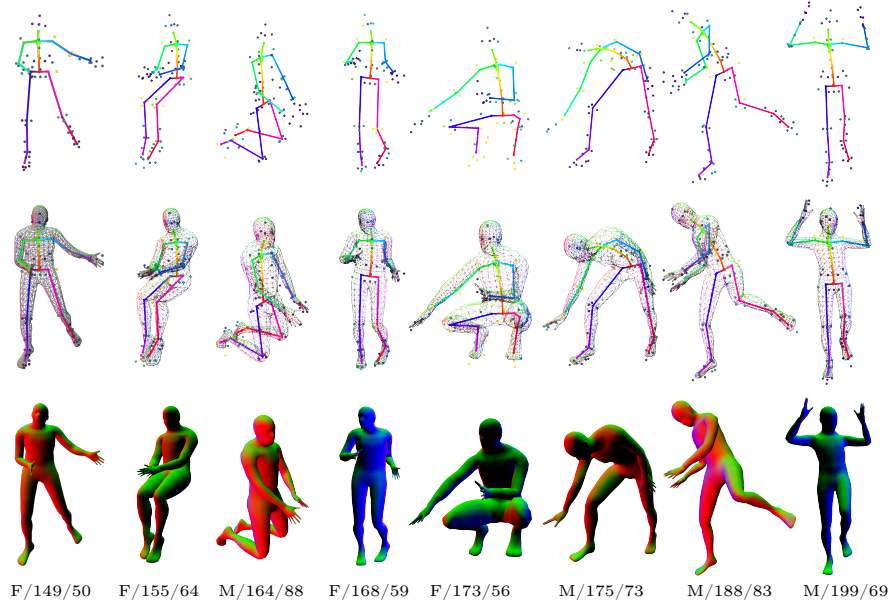


**Fig. 11: XSens retargetting for different body profiles.** Each column shows the fitting results of different body shape profile. This is specified by the bottom text, where the tuple  $X/Y/Z$  specifies a  $X$ -gender subject with  $Y$ cm height and  $Z$ Kg weight. The top row shows the XSens skeleton with 79 anatomical landmarks as defined in [62]. The landmarks are colored-coded by the fitting errors, with the darker color the lower error. The second row shows the retargetted mesh in polygons. The last row shows the same mesh rendered with normal shading.

**Tool interface.** To ground the narration, we develop the annotation tool to show annotators the synchronized videos of the egocentric RGB camera, the third-person RGB camera and the full-body motion rendered with scene point clouds. The tool interface is shown in Fig. 12. The tool allows annotators to segment the video into arbitrary length of clips. Then for each video segment, annotators write full-sentence answers to a set of predefined questions. We identify three annotation tasks to control the granularity from coarse to fine. The same tool interface is used to produce annotation for each tasks, where the questions are altered.

**Guidelines and narration questions.** We train annotators to identify the participants from the appearance of mocap suit and 3D rendering. Annotators are required to give clear descriptions as if they are describing the scenario over the phone for the recipient to reconstruct the scene. Annotators are asked to make reasonable segments that aligns with motion transition, and their descriptions should include all actions during that segment.

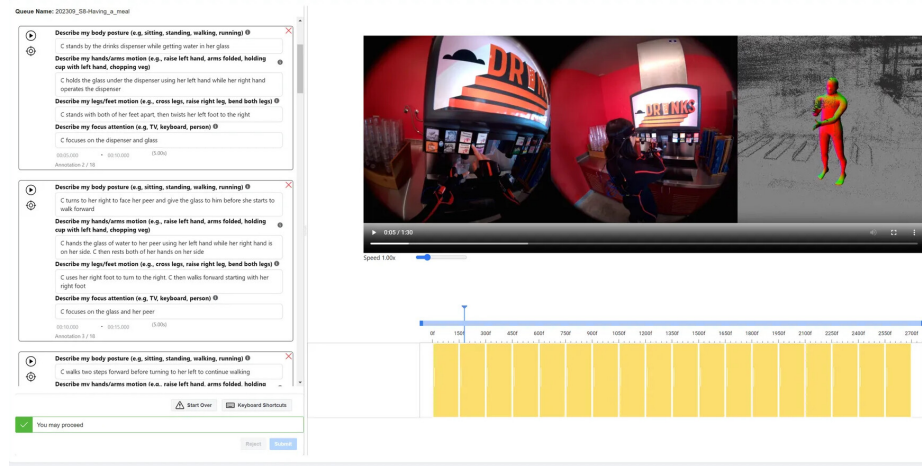


**Fig. 12: The narration tool interface.** Top right: annotators are presented with the synchronized egocentric RGB video, third-person RGB video and the rendering of the full-body motion. Bottom right: the video segmentation bar, where each yellow bar is one clip created by annotators to add description. Left: text boxes to enter answers to predefined questions. There is one text box per created segment. Following the Ego4D convention [29], participants are referred by C.

*Motion narration* is the finest level of annotation, which focuses on detailed body poses. For this task, each segment is between 3-5s long where annotators answer the following questions about the participants, *i.e.* 1) “describe the full-body motion including the direction/intent of the motion and environment”; 2) “describe the hands/arms motion”; 3) “describe the detailed legs/feet motion” and 4) “describe the focus attention”.

*Atomic actions* is the next level. For this task, segments are between 3-5s duration as well, however annotators only answer 1 question, *i.e.* “describe the actions, including body posture, direction/intend of motion, and interaction with objects and other people”. Compare to the previous task, annotators are encouraged to use verbs to describe actions whenever possible instead of focusing on body poses.

*Activity summarization* is the coarsest level of annotation, where annotators create segments of 15-30s duration and answer 1 question, *i.e.* “summarize the major activity, including the interaction with people/objects and the scene”.

## C Dataset Details

### C.1 Recording scenarios

**Definitions.** The Nymeria dataset defines 20 scenarios of daily indoor and outdoor motion. They are defined as follows.



script	i.d.	o.d.	2pt.	pct/%	dur./h	H/Km	L/Km	R/Km
S1 Relax at home	✓			2.40	9.02	2.97	3.11	3.59
S2 Where is X	✓		✓	9.80	36.87	30.25	37.90	41.49
S3 Welcome to my place	✓	✓	✓	5.00	18.80	57.94	64.89	66.44
S4 Body stretch	✓			2.00	7.62	22.80	27.93	26.92
S5 Cardio/workout	✓			2.20	8.39	5.03	8.42	8.68
S6 Dancing	✓			1.70	6.55	9.62	28.32	26.29
S7 Cooking	✓		✓	12.90	48.52	7.46	14.45	13.31
S8 Having a meal	✓	✓		4.45	16.73	33.35	41.03	47.47
S9 Making a mess	✓			1.83	6.90	14.09	15.18	15.21
S10 Housekeeping	✓		✓	6.80	25.57	8.98	12.19	13.24
S11 laundry and packing	✓			2.41	9.05	10.26	14.46	14.75
S12 Game night	✓		✓	10.39	39.08	21.60	22.90	29.58
S13 Charades	✓			2.43	9.15	7.47	14.63	15.27
S14 By the desk	✓			1.52	5.73	2.39	2.25	2.46
S15 Do as I command	✓			2.06	7.74	8.77	15.60	15.31
S16 Simon says	✓	✓		15.72	59.15	61.21	73.73	78.85
S17 In the office	✓			1.90	7.16	5.31	6.80	7.92
S18 Hike		✓	✓	2.77	10.44	27.33	30.68	30.50
S19 Fresh air		✓	✓	5.76	21.66	56.17	67.98	72.77
S20 Party time	✓		✓	5.86	22.04	17.87	21.84	24.20
sum	18	5	8	100.0	376.2	411.0	524.4	554.4

**Table 7: Summary of scenarios.** We mark scenarios for capturing indoor activities (i.d.), outdoor activities (o.d.), and two-participants collaborations (2pt). The recording hours and trajectory length is broke down by head(H), left wrist(L) and right wrist(R). The percentage of each scenario is computed from the overlapping recording time of all devices. The recording duration in this table also include time spent on eye calibrations at the start of each recording and additional data without low-quality motion. This is longer than 300 hours, which is the amount of clean data with all modalities.

- *S1 Relaxing at home.* In this script participants pretend to have a relaxing evening at home after work. The common activities include sitting on couch or laying on sofa to watch TV, finding books to read, looking for snacks or beverage to enjoy etc. Operators are instructed to prompt participants to change their activities if participants have been staying at one location for more than 5min.
- *S2 Where is X.* In this script, participants look for objects left behind in the house. The common activities include walking around the house, standing on toes or bending over to open cabinets and drawers, looking around, communicating with operators etc. Participants usually found 5 - 10 objects during a 15min recording. Operators are instructed to hide objects at places

where people commonly forgot them behind, *e.g.* phone under pillow, laptop next to nightstand, keys in jacket pockets, toys under the bed etc.

- *S3 Welcome to my home.* In this script, participants pretend to be the homeowners to give visitors a house tour. The common activities include greeting guests, offering beverages, walking around the house, having natural conversations etc. When there are two participants, they take turns to introduce different rooms. Operators and observers are instructed to prompt participants by asking for water, to see different rooms and questions about the house decorations etc.
- *S4 Body stretch.* In this script, participants follow video instruction to perform light body stretch exercises. We rotate different youtube videos to add some diversity. A common stretching exercise is yoga alike motion. We always confirm with participants for their comfortable level of exercising before proceeding.
- *S5 Cardio/workout.* Similar to S4, in this script participants follow video instruction to for workout sessions. Compare to S4 which is designed to record full body stretching, S5 captures faster body motions, *e.g.* jumping jacks, kicking feet back into a plank position, squatting etc. A few houses are equipped with indoor biking and treadmill, where participants are encouraged to leverage these workout tools instead of following videos. We always confirm with participants for their comfortable level of exercising prior to recording.
- *S6 Dancing.* Similar to S4 and S5, in this script participants mainly follow video instructions to dance. To capture the natural reactions, participants are not required to know how to dance prior to recording. we always confirm with participants for their comfortable level before proceeding. Compare to S4 and S5, S6 captures more frequent arm swings and body rotation. We choose multiple dancing videos to include salsa, cha cha cha, rumba etc.
- *S7 Cooking.* In this script, participants are provided with cooking ingredients to prepare a dish in the kitchen. The common activities include gathering ingredients from fridge, looking for tools, washing and chopping vegetables, stirring or frying with pans, seasoning, cleaning afterwards etc. The commonly used receipes for cooking include quesadilla, tacos, stir fry, baking, salad, BLT sandiches etc.
- *S8 Having a meal.* In this script, participants have lunch with operators. We capture this scenario at houses and in an large open-space cafeteria with outdoor patio. The common activities include setting table, getting food and drinks from buffet, having meal with friends, returning dishes, cleaning up table, load/unload dishwasher etc.
- *S9 Making a mess.* This script is defined for participants to create natural messy home. Typical activities include walking around the house, carrying objects and misplacing them, throwing stuff around etc.
- *S10 Housekeeping.* This script is usually done in combination with S9, where participants clean up the house. It is usually done by a different participant who created messy home before. The common activities include ordering objects, making bed, cleaning up floor etc.

- *S11 Laundry and packing.* In this script, participants are asked to do laundry and packing for travel. The common activities include folding clothes, load/unload washing machine, hanging up clothes, packing suitcase etc.
- *S12 Game night.* In this script, participants playing various games with other people. We also make use of existing entertaining facilities whenever possible. The common activities captured include playing poker, chess, gengar, boardgames, puzzles as well as fussball, pacman, pooling, mini golf, dart etc.
- *S13 Charades.* Similar to S12, this script is also defined for participants to play games with other people, however, the focus is to act with body language with participants being the performers. Depending on the characters of participants, either participants come up with various themes to act themselves for the operators to guess or participants are prompted by the operators. Operators are instructed to encourage participants to exaggerate their body language and move around.
- *S14 By the desk.* In this script, we focus on how people doing work from a working from home setup. To simulate the real-life scene, participants are often prompted to do computer-related tasks, *e.g.* typing speed test, solving online quiz, browsing websites etc. We also capture participants writing or doodling on a notebook and doing crafting such as origami.
- *S15 Do as I command.* This is the only script designed to cover a set of useful locomotion for algorithms to derive full-body pose prior instead of to understand natural daily activities. Participants are asked to act according to a predefined motion list, including walking, jogging, running, skipping, jumping etc on the spot, in a circle and backwards, rotating head/upper body/arms/ankle clockwise and anti-clockwise, kicking legs, bowling, touching toes, boxing, squatting, sitting down, taking stairs, lying flat etc.
- *S16 Simon says.* This script shares the same spirit of S15, where participants follow the instructions from operators to perform actions. However, the goal is tailored towards a mini real-life events, *e.g.* making tea, taking picture off the wall, measuring furniture, water plants, bring grocery from the car, picking flowers from the garden etc. As the name suggest, the scenario is inspired by the children’s game, where a person always uses the phrase “Simon says” to propose a action for everyone else to follow. This script helps us better capture the long-tailed daily activities that are otherwise difficult to incorporate into other recording scenarios. This is also one of the scenarios where audio records the psuedo ground truth of action labels.
- *S17 In the office.* This script is captured in an office building with multiple meeting rooms. Compare to S14, this scenario focuses on working onsite. The common activities include navigating in the building, taking stairs, having conversation at different locations, finding meeting spaces, giving presentations, using whiteboard, working on a laptop, taking breaks etc.
- *S18 Hike.* In this script, participants hike in the woods. We include multiple hiking trails with easy flat ones and median hilly ones.
- *S19 Fresh air.* This script focuses on outdoor refreshing activities, where participants typically play badminton, soccer, swing, jogging, or biking. We record most scenarios on a campus and in the backyard of houses.

- *S20 Party time.* This script is design for people to decorate a house for party or holiday celebrations. The common activities include making balloon (animals), setting up table, hanging decorations, arranging furniture etc. Most of our party scenario are recorded with two participants.

**Statistics.** The summary of recording statistics is given in Table 7. Note that the recording duration in Tab. 7 includes time spent on in-session eye calibration at the beginning of each recording and additional data where motion recording is poor quality. Therefore the summed value is longer than 300 hours, which is the amount of clean data with all modalities aligned with high-quality motion.

## C.2 Locations

The Nymeria dataset contains 50 locations, with 47 houses, 1 cafeteria with an outdoor patio, 1 multistory office building and 1 campus ground with parking lot and multiple hiking/biking trails. The last 3 locations covers different spaces of the same campus, where all recordings are aligned into the same world coordinates. To achieve this, we collected extra basemap recordings which connect the disjoint locations. We refer this merged location by BX. Table 8 present the details of each location, and the accumulated trajectory length per location. In addition to Fig. 5 in the main submission, Fig. 13 provides visualizations of more locations.

loc.	day	dur./h	H/Km	L/Km	R/Km	m.f.	type	liv.	k&d	other
AB02	4	4.32	2.50	3.61	3.53	✓	3b3b	2	1	yd.la.ga.re.
AB03	2	3.85	2.19	2.74	2.91	✓	3b1b	1	1	yd.la.
AB04	3	6.62	3.77	3.86	4.54		2b2b	1	1	yd.la.
AB05	2	3.87	2.51	3.02	3.22	✓	2b1b	1	2	yd.la.
AB06	3	4.94	4.35	4.84	5.58		3b2b	1	1	yd.
AB07	2	4.38	3.35	5.74	5.87		3b2b	1	1	yd.of.
AB08	3	6.74	6.41	11.0	11.7	✓	3b1b	1	1	yd.la.of.
AB10	3	7.74	4.66	7.78	7.90		1b1b	1	1	yd.la.
AB11	4	10.8	8.20	12.8	13.2	✓	3b2b	1	1	yd.
AB12	2	5.35	4.55	7.57	7.72	✓	3b3b	2	2	yd.la.
AB13	3	8.06	8.61	14.9	15.2		2b1b	1	2	
AB14	2	5.48	6.79	9.50	9.54		3b2b	1	1	yd.
AB15	3	6.67	6.10	8.74	8.97		3b2b	1	1	yd.la.re.
AB16	2	5.46	5.98	9.24	9.41	✓	5b3b	2	1	yd.la.of.ga.
AB17	3	7.47	6.69	11.7	11.0	✓	4b2.5b	1	2	
AB18	2	5.26	4.96	7.67	7.67		3b1b	1	1	yd.
AB19	2	5.20	3.97	6.50	6.70		3b2b	2	2	yd.la.ga.
AB20	3	6.80	5.92	8.93	9.58	✓	4b3b	1	1	yd.la.of.
AB21	2	5.45	4.69	8.36	8.31		2b1b	1	2	yd.la.

loc.	day	dur./h	H/Km	L/Km	R/Km	m.f.	type	liv.	k&d	other
AB22	3	7.88	8.15	11.8	12.5	✓	4b2b	1	2	yd.la.
AB23	2	4.00	3.58	4.78	5.14		3b2b	1	2	yd.
AB24	3	7.86	6.75	8.85	9.34	✓	5b2b	1	2	yd.
AB25	2	5.35	5.72	6.79	7.16	✓	4b2b	2	1	yd.
AB26	3	6.56	7.06	8.64	9.31	✓	4b3.5b	2	4	yd.la.ga.
AB27	2	3.95	3.93	4.60	5.07	✓	9b2.5b	1	2	yd.la.ga.re.
AB28	2	5.27	5.21	5.99	6.63		3b3b	2	2	yd.la.
AB29	3	8.01	8.68	10.9	11.2	✓	4b2b	1	2	yd.la.
AB30	2	5.41	5.75	6.87	7.55	✓	2b2b	1	2	
AB31	3	8.27	12.1	15.0	16.6	✓	5b2b	2	2	yd.la.ga.
AB32	2	5.12	7.09	7.76	8.91	✓	4b3b	1	2	yd.of.ga.
AB33	3	8.13	10.3	12.8	13.0	✓	4b2b	1	2	yd.re.
AB34	2	5.40	6.07	7.67	7.99	✓	4b4b	1	2	
AB35	3	8.15	9.02	10.4	10.8	✓	5b3b	1	2	
AB36	3	8.24	11.5	14.1	14.7	✓	5b3b	1	2	yd.la.
AB37	2	5.45	6.91	8.24	9.08	✓	4b2.5b	1	2	yd.la.re.
AB38	3	8.28	10.1	11.8	13.4		4b1.5b	1	2	yd.re.
AB39	2	4.11	3.75	4.28	5.11		4b2b	1	2	yd.la.
AB40*	4	15.3	14.0	16.7	17.8	✓	4b3b	2	3	yd.la.re.
AB41	3	7.74	8.08	9.40	10.9	✓	4b3.5b	1	2	yd.la.of.
AB42	2	5.45	5.82	6.60	8.03	✓	4b3b	1	2	yd.
AB43*	3	7.73	7.34	8.40	9.32		5b2b	2	1	yd.
AB44*	2	8.24	7.12	8.20	9.16	✓	5b2b	2	3	yd.
AB45*	3	12.9	9.20	11.6	12.7		2b2b	1	2	yd.la.
AB46*	2	8.52	6.76	8.01	8.73	✓	6b3.5b	1	1	yd.la.of.
AB47*	3	11.8	12.1	15.8	17.0	✓	4b2.5b	1	1	yd.la.of.
AB48*	2	6.30	4.95	5.96	6.78	✓	3b2b	1	1	yd.
AB49*	3	12.9	12.98	15.88	16.8	✓	3b3b	1	1	yd.la.re.of.
BX*	20	50.9	94.53	107.8	110.9	✓				
sum	122	377.8	411.0	524.4	554.4	32		58	79	

**Table 8: Summary of locations.** For each location, we report the number of days spent onsite, the recorded data duration in hour, the trajectory lengths in Km of head(H), left wrist(L) and right wrist(R), respectively. The table also summarizes the location layout. The prefix AB indicates houses and the location BX combines 3 areas on a large campus. Locations marked with \* contain two-participant collections. The abbreviations have the following meanings: XbYb for X bedrooms and Y bathrooms, m.f. for multi-floor, liv. for living room, k&d for kitchen and dinning space, yd. for yard, la. for laundry room, ga. for garage, re. for recreation room, and of. for office room. Note the summed hour is longer than 300 for the same reason given in Table 7.

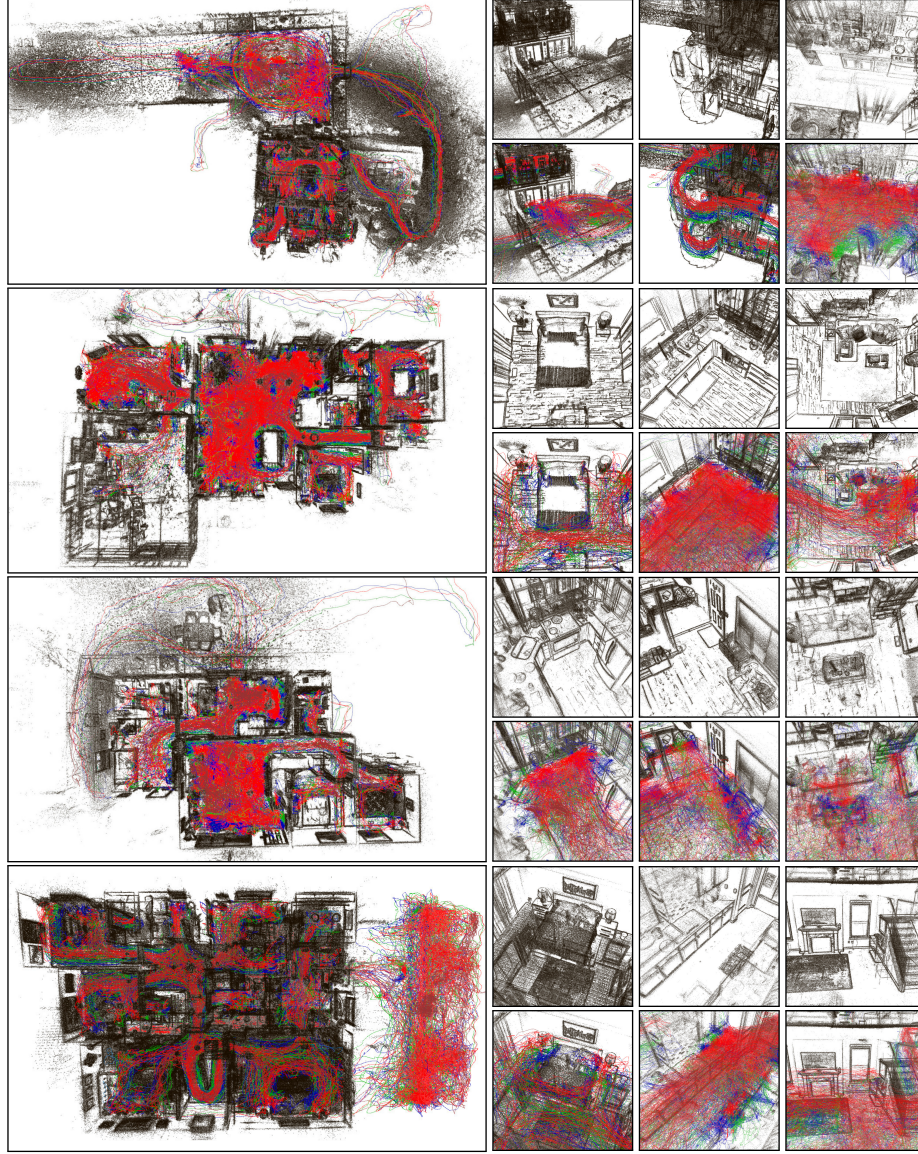


**Fig. 13: Additional visualization of the MPS output for multiple recording locations from the Nymeria dataset.** Left: map and all trajectories aligned in it. Right: zoomed-in locations within the map, with and without trajectories. The observer and participant head trajectory is shown in red, and the left and right wrist trajectory are shown in green and blue respectively.



## D Benchmarks

In this section we provide details about how baseline methods are trained and evaluated with our dataset. We also provide qualitative results of the baseline algorithms in addition to the quantitative evaluations reported in the main submission.

### D.1 Baseline methods

**AvatarPoser.** AvatarPoser [40] is a regressive method based on the transformer architecture. It takes positional information about 3 body joints (head and hands) for the last 40 frames (0.66s) and outputs full-body pose prediction for the last frame in a form of local rotations for each joint. The translation of the body is then inferred by using the input head joint position and traversing it up the kinematic chain to the model’s root joint. The model does not predict the shape of the body and uses GT shape parameters to infer the position of the joints. The input positional information is encoded as a vector of the translation, rotation and linear and angular velocity of head and hands. Original model assumes SMPL [52] body model; to benchmark the method on our dataset, we adapted the inference pipeline to work with the Xsens kinematic tree and increased the number of predicted joints from 22 to 23; otherwise, we tried to maintain the original pipeline intact, reusing the original preprocessing and training scripts, and retrained the model from scratch.

**BoDiffusion.** BoDiffusion [16] is a 3-point to full-body motion generation method based on a Diffusion framework. The method takes a sequence of 3 point information frames and produces a window of full-body motions. BoDiffusion uses same input and output representations as AvatarPoser, sharing similar data preprocessing and motion inference pipelines. The architecture used in BoDiffusion is DiT [69] – a Transformer-based architecture with global conditioning. Similar to AvatarPoser, we only modified the inference method to work with the Xsens skeleton and changed the output size, keeping other parts original. We retrained the model from scratch on our data – it took about 3 times longer to converge on our data compared to AMASS.

**EgoEgo.** EgoEgo [48] method is a diffusion-based method which predicts the full-body motion from head-mounted camera images. It has a two-stage pipeline: the first stage is a visual localization network, predicting the head trajectory from a series of camera images. The second part is a diffusion-based method which generates the full-body motion given the head trajectory predicted on the previous stage. Since the localization of our SLAM system is very robust, we are only interested in benchmarking the performance of the full-body prediction stage, therefore we dropped the visual localization stage and supplied the head positions to the diffusion-based model directly. Similar to the other baselines, we adapted the method to work with Xsens skeleton instead of SMPL, keeping



the original architecture of the model. To train the model from scratch we used BoDiffusion diffusion training pipeline and code base as it was easier to adapt for our data.

**VQ-VAE.** VQ-VAE [24, 64] encodes high-dimensional data into discrete latent codes. With the large amount of motion data in this dataset, we are able to train a VQ-VAE that encodes motion representations into sequences of motion tokens, which has wide applications in motion generation and understanding [32, 38, 98]. To train the VQ-VAE, we first represent human motions as sequences of poses and root joint translation velocity and rotation. Each pose is represented by joint angles and joint rotation velocity defined on a kinematic tree. The motion VQ-VAE consists of fully convolutional encoder and decoder, which makes it capable of processing motions with arbitrary lengths. Both the encoder and decoder comprise three layers of 1-D convolution residual blocks. For the latent quantization, we use three techniques, including exponential moving average, codebook reset [24] and product quantization [53], to improve the codebook usage rate and expressiveness, which are important to the reconstruction performance. For training, we use motion batches with window size of 1 second, which is equivalent to 60 frames under 60 fps.

**TM2T.** TM2T [32] is one of the early attempts that encodes motions into discrete tokens and use transformers for the generation and understanding of motions. The method first trains a motion VQ-VAE to map contiguous motion representations into discrete motion tokens. Then a transformer-based architecture is trained to map motion tokens to language tokens for motion understanding, or the other around for text-to-motion generation. To benchmark the method on our dataset, we use the motion VQ-VAE described above as the motion tokenizer. We adopt GPT-2 [74] tokenizer for motion narration tokenization. For each motion segment, we stack the motion narration for full body, upper body and lower body together to form the target motion narration. We are interested in the motion understanding part of the work. Therefore, we train the motion-to-text generation as the motion understanding baseline, using the official codes.

**MotionGPT.** MotionGPT [38] uses language models to establish the joint distribution of motion and language so that the model can be prompted with natural languages for different motion tasks, *e.g.*, motion prediction, motion in-between, text-to-motion generation, motion understanding. Similarly, MotionGPT also trains a motion VQ-VAE to tokenize the motions. Then to establish the joint distribution, MotionGPT starts from a pre-trained language model T5 [75] and trains with motion-to-text and text-to-motion translation tasks as the second stage. Lastly, instruction tuning is performed to prompt the model for different downstream tasks. Similar to TM2T, we test motion understanding on MotionGPT with our dataset. We use the same VQ-VAE described above as the motion tokenizer. We use the official codes and perform the second stage training

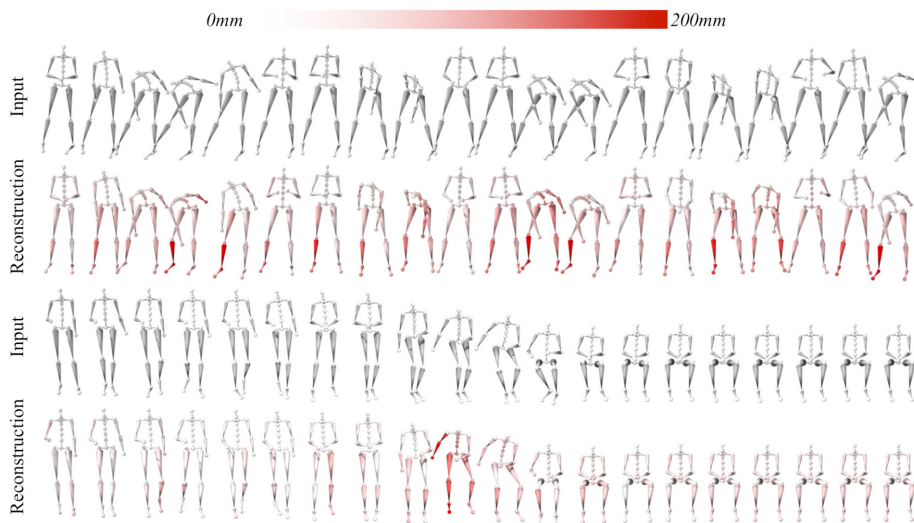


**Fig. 14: VQ-VAE motion reconstruction.** This visualization is produced by the best VQ-VAE we trained, which corresponds to the last line of main paper Tab. 4.

with motion-to-text and text-to-motion tasks. Then we directly use the model from this stage to test motion understanding.

## E Contributions and Acknowledgements

**Contribution.** Lingni Ma led the project, developed the pipeline to construct the dataset, coordinated data collection/processing, and led the baseline evaluations. Yuting Ye developed the solution for human motion retargetting, advised data collection and evaluations. Fangzhou Hong, Vladimir Guozv and Yifeng Jiang, validated the dataset and implemented baselines. Rowan Postyeni supported daily operations, processed XSens motion data and performed quality assessment for XSens motion and narration. Luis Pesqueria served the program manager for data collection and narration. Alexander Gamino was responsible for multi-device tracking. Vijay Baiyya was responsible to Project Aria MPS scaled processing. Hyo Jin Kim supported narration annotations. Kevin Bailey and David Soriano Fosas lead hardware development of miniAria wristband. C. Karen Liu and Ziwei Liu acted as technical advisor to data collection, annotation and baseline evaluations. Jakob Engel, Renzo De Nardi and Richard Newcombe were the senior technical and scientific advisors.

**Acknowledgement.** We gratefully acknowledge the following colleagues for their valuable discussions and technical support. Genesis Mendoza, Jacob Alibadi, Ivan Soeria-Atmadja, Elena Shchetinina, and Atishi Bali worked on data collection. Yusuf Mansour supported gaze estimation on Project Aria. Ahmed

Elabbasy, Guru Somasundaram, Omkar Pakhi, and Nikhil Raina supported EgoBlur as the solution to anonymize video and explored bounding box annotation. Evgeniy Oleinik, Maien Hamed, and Mark Schwesinger supported onboarding Nymeria dataset into Project Aria dataset online browser. Melissa Hebra helped with coordinating narration annotation. Tassos Mourikis, Maurizio Monge, David Caruso, Duncan Frost, and Harry Lanaras provided technical support for SLAM. Daniel DeTone, Dan Barnes, Raul Mur Artal, Thomas Whelan, and Austin Kukay provided valuable discussions on annotating semantic bounding box. Julian Nubert adopted the dataset for early dogfooding. Pedro Cancel Rivera, Gustavo Solaira, Yang Lou, and Yuyang Zou provided support from Project Aria program. Edward Miller served as research program manager. Pierre Moulon provided valuable guidance to opensource codebase. Svetoslav Kolev provided frequent feedbacks. Arjang Talattof supported MPS. Gerard Pons-Moll served as senior advisor. Carl Ren and Mingfei Yan served the role of senior managers.

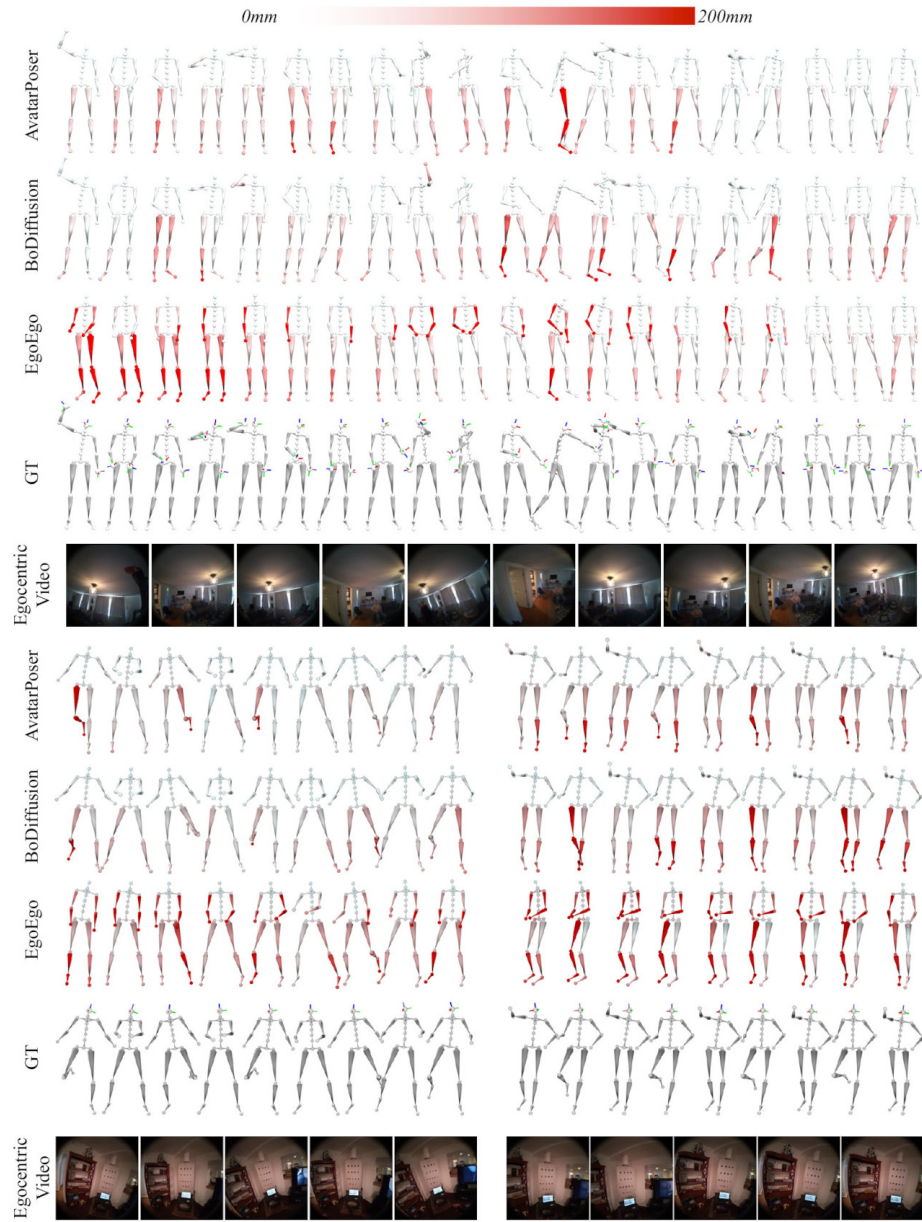
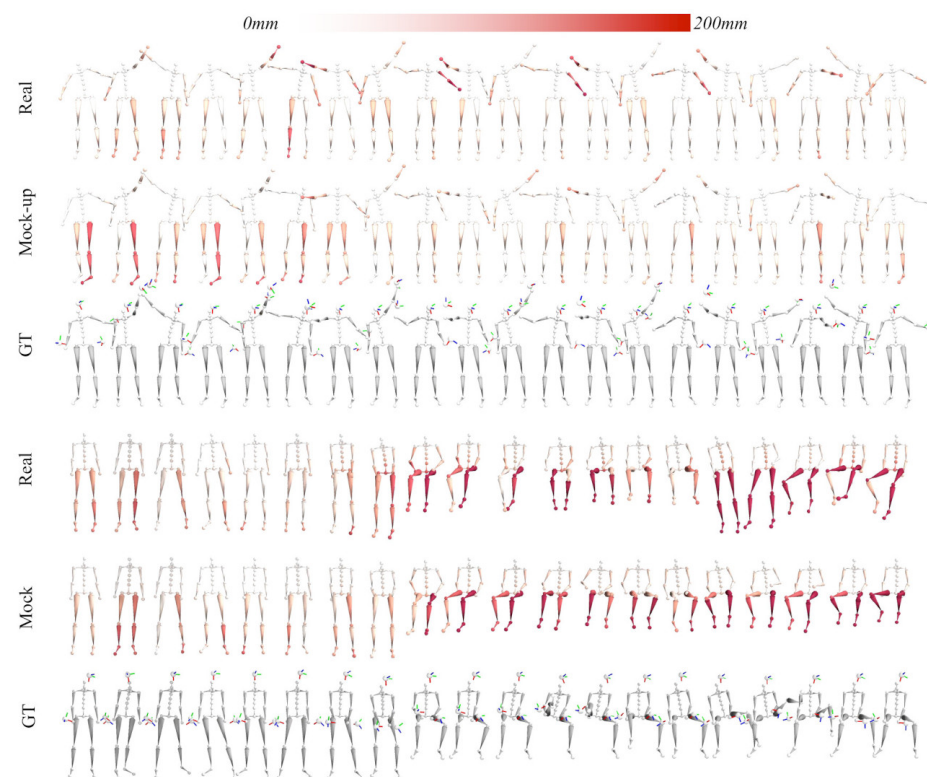


Fig. 15: Full-body tracking from 3-point and 1-point motion input.



**Fig. 16: Full-body tracking from real 3-points v.s. mock-up 3-points.**



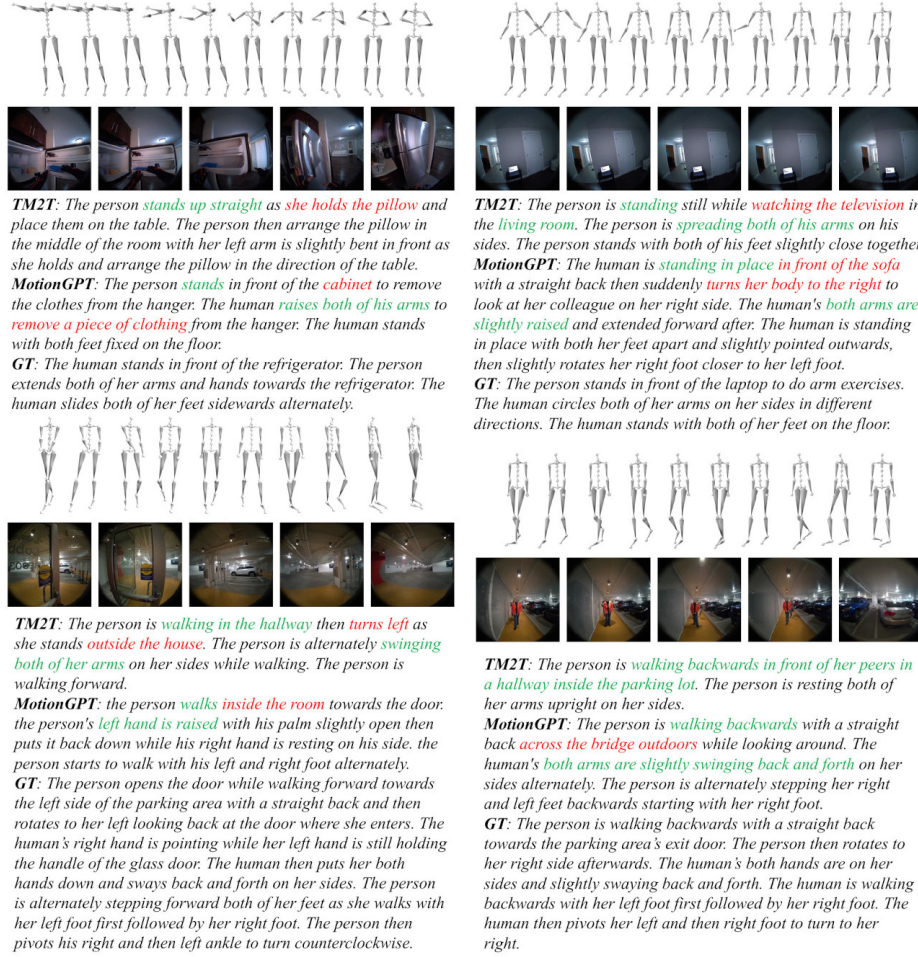


Fig. 17: Motion understanding from 3-point input.